Effect of Unsaturated Bonds on NOx and PAH Emissions of Triple Flames

By Xu Han

M.S. Mechanical Engineering

University of Illinois at Chicago, Chicago, 2012

THESIS

Submitted as partial fulfillment of the requirements

for the degree of Master of Science in Mechanical Engineering

in the Graduate College of the

University of Illinois at Chicago, 2012

Chicago, Illinois

Defense Committee:

Dr. S.K. Aggarwal, Chair and Advisor

Dr. Kenneth Brezinsky

Dr. Rodica Baranescu

To my parents Meiying He and Guozhu Han, and all my friends.

ACKNOWLEDGMENTS

First, I would like to express my gratitude to my advisor, Professor S.K. Aggarwal, for all the help, instruction, and support. It is him who contributed so much to this work. Thank him also for all the opportunities I got. Attending the Central State Conference is such a nice memory. I would also like to appreciate Professor Kenneth Brezinsky who also helped and supported me on my study. Without his leading me to this fascinating field, and his financial support and trust, I cannot get this far. Thank Professor Rodica Baranescu for agreeing to be part of my committee and be willing to support me in the future.

I would like to acknowledge Xiao Fu for all the help in these two years. Thank Arun Sebastian, Sudhanshu Jain, and Dylan Lawson for all the philosophical talks that make the most interesting part of life. Thank Hwansoo Chong, Donglu Li, and all my colleagues from the Flow and Combustion Simulation Laboratory and the High Pressure Shock Tube Laboratory, for all the help and great time I had.

At last, I want to express my special thanks to my parents for all the support they gave me.

Table of Contents

List of Figures

List of Tables

Summary

Various engine and shock tube studies have reported increased NO_x emissions from the combustion of biodiesels than from regular diesel, and linked it to the degree of unsaturation or the number of double bonds in the molecular structure of long chain biodiesel fuels. We report herein a numerical investigation on the structure and emission characteristics of triple flames burning saturated and unsaturated surrogate diesel fuels. The surrogate fuels include n-heptane, 1-heptene, methyl decanoate, and methyl decenoates, N-heptane and 1-heptene represent, respectively, the hydrocarbon side chain of the saturated (methyl octanoate) and unsaturated (methyl octenoate) biodiesel surrogates. The other two C10 methyl esters have close chemical kinetics to real biodiesel fuels, which usually consist of heavy methyl esters. Our objective is to examine the effect of unsaturated (double) bond on NO_x and soot emissions in a flame environment containing regions of lean premixed, rich premixed and non-premixed combustion. For n-heptane and 1-heptene study, which is the main part of this work, a validated detailed kinetic model with 198 species and 4932 reactions was used to simulate triple flames in a counterflow configuration with different levels of premixing and strain rates. Results indicate while while the global structures of n-heptane and 1-heptene triple flames are quite similar, there are significant differences with respect to NO_x and PAH (polycyclic aromatic hydrocarbons) emissions from these flames. The NO_x production rates in the rich premixed, lean premixed, and non-premixed zones are higher in 1-heptene flames than in n-heptane flames, and the differences become more pronounced as the level of premixing is increased. The NO_x formed through the prompt, thermal, N_2O, and NNH mechanisms is also higher in 1-heptene flames. NO_x formation in the rich premixed zone is primarily due to the prompt NO, that in the nonpremixed zone is through the thermal NO, and that in the lean premixed zone is due to the NNH and N_2O routes. The PAH species are mainly formed in the rich premixed zone, and their emissions are significantly higher in 1-heptene flames than in n-heptane flames. The reaction pathway analysis indicated that the dominant path

for benzene formation involves the combination of two propargyl (C_3H_3) radicals, and the presence of double bond in 1-heptene provides a significant route for its production through the formation of C_3H_5. This path is not favored in the oxidation of n-heptane, as it decomposes directly to smaller alkyl radicals. While the NO_x and PAH emissions decrease with the increase in strain rate, they are consistently higher in 1-heptne flames than in -heptane flames, irrespective of the strain rate. For the study of methyl decanoate and methyl decenoates, reduced mechanism recently developed by three different institutions was used. The result shows that the effect of unsaturated bond on NO_x emissions in methyl esters is similar to that in long alkene hydrocarbons.

1. Introduction

1.1 Background

Biodiesel fuels have attracted significant interest due to their potential as a renewable fuel. Moreover, numerous flame and engine studies[1,2] have reported noticeable reduction in the emissions of CO, unburned hydrocarbons, and particulate matter from the combustion of biodiesel fuels compared to those from conventional diesel, although NO_x emission has generally been found to increase. Some recent investigations have focused on identifying the chemical and physical processes associated with this increased NO_x. An important characteristic of biodiesels, produced from the transesterification of vegetable oils and animal fat, is the existence of double and triple bonds in their molecular structure. The chain length and unsaturated bonds in the fuel molecular structure are known to have a significant influence on the fuel combustion chemistry, and thereby on the combustion characteristics, including ignition delay, flame speed, and pollutant emissions.

McCormick et al.[3] performed engine tests using several biodiesel fuels from different feedstock, and observed higher NOx emissions as the fatty acid chain length and the number of double bonds were increased, although there was no significant change in PM emissions. In contrast, Lapuerta et al.[4] observed noticeable reduction in PM emissions with the number of double bonds or degree of unsaturation in the fuel molecular structure, while Puhan et al.[5] reported increased emissions of NOx, smoke, CO and unburned hydrocarbons (UHCs) with the degree of unsaturation, based on their single-cylinder engine experiments with linseed, jatropha and coconut oils. Schönborn et al.[6] reported similar results for fatty acid alkyl esters, i.e., higher PM emissions with the increase in the number of double bonds. Benjumea et al.[7] conducted single-cylinder engine experiments with three different mixtures of

fatty acid methyl esters, and showed that smoke opacity, and emissions of NOx and UHC increased with the degree of unsaturation. In addition, a higher degree of unsaturation was found to increase the ignition delay and retard the start of combustion, which is also expected to influence the PM and NOx emissions. Salamanca et al.[8] examined the effects of chemical composition and the degree of unsaturation of methyl esters on engine emissions, and observed that linseed biodiesel produced more PM and UHC than Palm biodiesel as a consequence of more unsaturated compounds in its composition, which favor the formation of soot precursors in the combustion zone.

There have also been fundamental studies on the effect of unsaturated bonds on NOx and PAH (polycyclic aromatic hydrocarbons) formation. Garner et al.[9,10] performed shock tube experiments on the pyrolysis and oxidation of n-heptane (n-C_7H_{16}), 1-heptene (C_7H_{14}-1), methyl octanoate (C9:0), and methyl trans-2-octenoate (C9:1) fuels, and observed that higher NO can be related to the presence of double bonds in the molecular structure of unsaturated fuels, namely, 1-heptene and methyl octenoate. Note that n-heptane and 1-heptene represent, respectively, the hydrocarbon side chain of the surrogate bio-diesel esters, methyl-octanoate and methyl-octenoate. Using detailed kinetic models, Garner et al.[11] further demonstrated the coupling between the increased acetylene (C_2H_2), formed from unsaturated fuels, and the higher prompt NO formed under fuel rich conditions. Acetylene is also a good precursor for PAH and soot formation. Sarathy at el.[12] compared two fatty acid methyl esters, methyl butanoate and its unsaturated counterpart methyl crotonate, in opposed flow diffusion flame and jet stirred reactor. Methyl crotonate was observed to produce higher C_2H_2, 1-C_3H_4, 1-C_4H_8, 1,3- C_4H_6 and benzene, indicating the potential of increased soot formation with unsaturated biodiesel fuels compared to the saturated ones, although soot emission is reduced with biodiesel compared to petrodiesel due to the presence of oxygen in biodiesel, and significantly higher amount of aromatics in petrodiesel.

To summarize, previous engine studies using various biodiesel fuels report a correlation between the increased NOx emissions and the degree of unsaturation in the fuel molecular structure. However, they

provide conflicting results concerning the effect of unsaturated bonds on soot emissions. This may be due to the strong coupling of various physical and chemical effects caused by the presence of unsaturated bonds. For instance, the fuel chemical structure is known to influence the fuel injection, atomization, vaporization and ignition delay processes in diesel engines, and consequently their combustion and emission characteristics. This underlines the need for more fundamental studies so as to isolate the effects of unsaturated bonds on NOx and soot emissions. While there have been investigations examining the chemical consequence of unsaturated bonds, their observations have been specific to highly diluted, homogeneous fuel-air mixtures, typical of shock tube and jet stirred reactor environment. Relatively little work has been reported dealing with these aspects in well-characterized flame environments. Fu et al.[13] reported a numerical investigation on NOx emissions in n-heptane and 1-heptene partially premixed double flames. Results indicated that the beta scission and oxidation reactions related to the double C=C bond lead to increased NO formation in 1-heptene flames than in n-heptane flames. Moreover, differences in the NO formation between the two fuels were found to be more pronounced as the level of partial premixing was increased. Analysis of the NO production pathways indicated that the NO is formed mainly though the prompt NO and N_2O intermediate mechanisms, rather than through the thermal and NNH mechanisms. PAH and soot emission is also expected to be higher from unsaturated bonds due to the important role of C_2H_2 in the formation of PAH species through HACA (hydrogen abstraction acetylene addition) mechanism.

The present work extends the above study to examine the effect of the presence of a double bond on both NOx and PAH formation in triple flames burning prevaporized n-heptane and 1-heptene fuels. The study is motivated by several considerations. The first is that fundamental flame investigations dealing with large hydrocarbons have mostly considered saturated fuels, such as heptane[14,15,16,17,18]. Another motivation is due to the importance of triple flames in numerous practical applications. Such flames play a fundamental role in characterizing lifted jet flames[19,20,21], as well as the propagation and stabilization of laminar and turbulent flames[22,23]. Such flames are also relevant to diesel engine combustion, especially in

the context of novel low temperature combustion concepts, including HCCI[24] (Homogeneous Charge Compression Ignition), PCCI[25] (Premixed Charge Compression Ignition), and dual-fuel injection. While triple flames burning smaller hydrocarbon fuels have been extensively investigated, there have been few studies dealing with large hydrocarbon fuels. Guo and Smallwood[16] numerically investigated n-heptane triple flames and observed that a large amount of prompt NO is formed in the rich premixed flame branch. They also discussed interactions involving heat and species transport between the three reaction zones. Briones et al.[26] investigated these interactions and their effects on NO_x emissions in methane-air double and triple flames, and concluded that triple flames may have an advantage in reducing NO_x emission over the corresponding premixed flames and double flames.

Furthermore, we also simulated diffusion flames and triple flames of methyl decanoate and methyl decenoates fuels. C10 methyl esters are surrogate fuels whose combustion chemistry is very similar to actual biodiesels.[27] And C10 methyl esters' molecules have a relatively close carbon number to the methyl esters species that form soy- and rapseed derived biodiesels (C16, C19 methyl esters). Methyl decanoate has a cetane number of 47, which is close to conventional diesel. In contrary to the study on heptene, this time, two isomers, methyl-2-decenoate and methyl-9-decenoate are chosen for the study of methyl decenoate. Although they have the same alkene side chain, but their chemical kinetics have difference, due to the relative position of the double bond from the methyl ester group. It is well known that this can affect ignition delay and fuel reactivity. But its effect on NO emissions is unclear. This study is aimed at improving our understanding of NO emissions of unsaturated methyl ester isomers. However, due to limitation of time and the complexity of the chemical kinetics of methyl decanoate and methyl decenoates, the in-depth discussions are left for future study.

In this paper, the triple flame structure is chosen for flame study. A triple flame is characterized by the existence of lean premixed, rich premixed, and non-premixed reaction zones, which are spatially separated but strongly coupled through the transport and chemical kinetic. Therefore, our major objective

is to elucidate the effect of the presence of double bond on NO_x and PAH emissions in partially premixed flames containing regions of lean premixed, rich premixed and nonpremixed combustion. Moreover, using a counter-flow geometry, the spatial separation between the three reaction zones can be controlled by varying the strain rate, and the lean and rich equivalence ratios. Consequently, this configuration facilitated a detailed analysis of NOx and PAH formation processes in each of the three reaction zones. Therefore, the relative contributions of prompt, thermal, N_2O intermediate, and NNH mechanisms to total NOx were also characterized by analyzing the production pathways in the three reaction zones.

2. **Physical-Numerical Model**

2.1 Physical description of counter-flow flame

Counterflow configuration is frequently applied for fundamental studies of flames and combustion chemistry. The configuration involves two opposing jets, which forms a stagnation plane between the two nozzles, as shown in Figure 1. One flat flame or more are stabilized after steady state is achieved. When one jet flow carries the oxidizer, while the other carries the fuel, then a diffusion flame is formed. When the fuel nozzle emits premixed fuel/air mixture, a partially premixed double flame can be formed, and it consists of one premixed flame and one diffusion flame. When one nozzle emits a lean premixed mixture while the other emits a rich premixed mixture, a triple flame can be formed, which consists of two premixed flames and a diffusion flame between them, as shown in Figure 1, and this is the type of flame we extensively study. Another type of counter-flow flame is the premixed counter-flow flame, which is formed by two lean premixed mixtures or two rich premixed mixtures. If the two premixed mixtures have exactly the same properties, composition, and speed, then it's called twin flame, which can be used for flame speed calculation. For counterflow flames, our focus is usually on the axis of this configuration, where the radial coordinate is zero. Thus, the fluid dynamics governing equations of the model can all be reduced to 1-D equations. The following gives the equations governing the fluid dynamics of counter-flow flame.

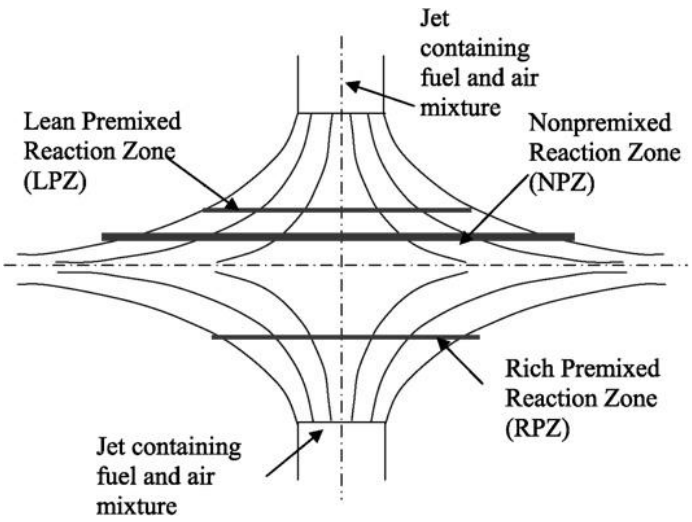

Figure 1: Counter-flow triple flame[26].

At steady sate, the mass conservation equation in cylindrical coordinate can be written as:

$$\frac{\partial(\rho u)}{\partial x}+\frac{1}{r}\frac{\partial(\rho v_r r)}{\partial r}=0 \tag{1}$$

Where ρ, u, v_r, x, and r are the density of the gas, axial velocity, radial velocity, axial position, and radial position. According to von Karman, it can be assumed that ρ and v_r/r are both independent of the radial position r. Thus, if we define

$$G(x)=-\frac{(\rho v_r)}{r} \qquad F(x)=\frac{\rho u}{2} \tag{2}$$

then we have

$$G(x)=\frac{dF(x)}{dx} \tag{3}$$

If we also define

$$H = \frac{1}{r}\frac{\partial p}{\partial r} \tag{4}$$

The momentum conservation equation is:

$$H - (n-1)\frac{d}{dx}\left(\frac{FG}{\rho}\right) + \frac{nG^2}{\rho} + \frac{d}{dx}\left[\mu\frac{d}{dx}\left(\frac{G}{\rho}\right)\right] = 0 \tag{5}$$

The energy conservation equation is,

$$\rho u\frac{dT}{dx} - \frac{1}{c_p}\frac{d}{dx}\left(\lambda\frac{dT}{dx}\right) + \frac{\rho}{c_p}\sum_k c_{p,k}Y_k V_k\frac{dT}{dx} + \frac{1}{c_p}\sum_k h_k\dot{\omega}_k + \frac{1}{c_p}\dot{Q}_{rad} = 0 \tag{6}$$

where Y, c_p, h, $\dot{\omega}$, V, and $\dot{Q}_{rad}$ are the mass fraction, specific heat, absolute enthalpy, species production rate, diffusivity, and heat loss due to radiation.

The species conservation equation is:

$$\rho u\frac{dY_k}{dx} + \frac{d}{dx}(\rho Y_k V_k) - \dot{\omega}_k W_k = 0 \qquad k = 1,...,K \tag{7}$$

The boundary conditions are given as,

$$x = 0: \quad F = \frac{\rho_F u_F}{2}; \quad G = 0; \quad T = T_F; \quad \rho u Y_k + \rho Y_k V_k = (\rho u Y_k)_F \tag{8}$$

$$x = L: \quad F = \frac{\rho_O u_O}{2}; \quad G = 0; \quad T = T_O; \quad \rho u Y_k + \rho Y_k V_k = (\rho u Y_k)_O \tag{9}$$

where subscript F and O represents the fuel nozzle and oxidizer nozzle in the diffusion flame case, respectively.

Equations (3-8) and the boundary condition (9) forms a simplified problem for the counterflow flame. The variables ω, Q_{rad}, c_p, μ, and V are achieved by thermodynamic data and transport data, or expressed by other equations.

We use mixture averaged formulation for the diffusivity V, which is

$$V_k = -\frac{1}{X_k} D_{km} \frac{dX_k}{dx} - \frac{D_k^T}{\rho Y_k} \frac{1}{T} \frac{dT}{dx} \qquad (10), \qquad \text{where } D_{km} = \frac{1 - Y_k}{\sum_{j \neq k}^{K} \frac{X_j}{D_{jk}}} \qquad (11)$$

D_{km}, D_{jk}, and D_k^T are the mixture-averaged, binary, and thermal diffusion coefficients, respectively. In our case, the thermal diffusion is neglected.

The reaction rate $\dot{\omega}$ is expressed by

$$\dot{\omega}_k = \sum_{i=1}^{I} \nu_{ki} q_i \qquad (k = 1, ..., K) \qquad (12)$$

where

$$\nu_{ki} = \nu''_{ki} - \nu'_{ki}$$

$$q_i = k_{fi} \prod_{k=1}^{K} [X_k]^{\nu'_{ki}} - k_{ri} \prod_{k=1}^{K} [X_k]^{\nu''_{ki}} \qquad (13)$$

k_f and k_r are the forward reaction rate and reverse reaction rate of a reaction, respectively. k_f is given by

$$k_{fi} = A_i T^{\beta_i} \exp\left(\frac{-E_i}{R_u T}\right) \qquad (14)$$

Most of the time, A, β, and E are not given for the reverse reaction. It is rather derived by

$$k_{ri} = \frac{k_{fi}}{K_{ci}} \tag{15}$$

where K_{ci} is the equilibrium constant of the reaction, and can be expressed as,

$$K_{ci} = K_{pi}\left(\frac{P}{RT}\right)^{\sum_{k=1}^{K} v_{ki}} \tag{16}$$

The equilibrium constants K_{pi} can be achieved by,

$$K_{pi} = \exp\left(\frac{\Delta S_i^o}{R} - \frac{\Delta H_i^o}{RT}\right) \tag{17}$$

where ΔS_i^o is the total entropy change through the reaction, and ΔH_i^o is the total enthalpy change through the reaction. Molar entropy and enthalpy of species can be achieved from the thermodynamic properties.

2.2 Numerical Simulation

N-heptane and 1-heptane triple flames in a counterflow configuration were simulated using the Chemkin and OPPDIF packages.[28,29] The configuration involves two opposing jets, one issuing a fuel lean mixture and the other a fuel rich mixture. The triple flame structure and the spatial separation between the three reaction zones are controlled by varying the global strain rate and the fuel-lean (Φ_L) and fuel-rich (Φ_R) equivalence ratios. The global strain rate is defined as

$$a_g = \frac{2v_R}{L}\left(1 + \frac{v_L\sqrt{\rho_L}}{v_R\sqrt{\rho_R}}\right) \tag{18}$$

Here v_R, and v_L denote, respectively, the inlet flow velocities of the rich and lean streams, and L is the distance between the two nozzles. Since the gravitational effect is not considered, rich and lean mixtures

can be introduced from either nozzle. In the present study, the fuel-lean mixture is issuing from the left nozzle, and fuel-rich mixture from the right nozzle. In addition, L is taken as 2cm, the pressure as one 1atm, and the temperature of both the streams as 400K.

The kinetic mechanism used to model the n-heptane and 1-heptene oxidation chemistry is due to Ranzi et al.[30,31]. The mechanism has been previously validated by Shimizu et al.[32] and Frassoldati et al.[33]. The NOx formation is modeled using the detailed thermal, prompt, N_2O intermediate, and NNH intermediate mechanisms.[34,35] Details are provided in an earlier study[13]. The combined fuel oxidation and NOx formation mechanism consists of 198 species and 4932 reactions. As discussed in the cited studies, thermal NO route is important at high temperatures (above 1800K), while prompt NO is relevant in rich flames over a wide temperature range. The N_2O and NNH routes have been found to be important under low-temperature conditions.[36,37,38,39,40] Löffler et al.[38] studied natural gas combustion and found that N_2O route is important under lean conditions at temperatures below 1600K, while NNH route is important under rich conditions due to high H radical concentration. Konnov et al.[41] simulated hydrogen combustion in well stirred reactors and observed that the NNH route is also important under lean and stoichiometric conditions at 1500K.

In order to quantify the relative contributions of various NO mechanisms, we isolated each mechanism by removing the initiating reactions associated with the other three mechanisms. The initiating reactions are the ones in which nitrogen reacts directly to form the relevant species. Thus the initiating reaction for thermal NO is

$$N_2 + O \Leftrightarrow N + NO \qquad (\#1)$$

The main initiating reactions for prompt NO are

$$CH + N_2 \Leftrightarrow HCN + N \qquad (\#2)$$

$$CH_2 + N_2 \Leftrightarrow HCN + NH \qquad (\#3)$$

$C + N_2 \Leftrightarrow CN + N$ (#4)

The main initiating reactions for N_2O intermediate mechanism are

$N_2 + O (+M) \Leftrightarrow N_2O (+M)$ (#5)

$N_2O + H \Leftrightarrow N_2 + OH$ (#6)

$N_2O + O \Leftrightarrow N_2 + O_2$ (#7)

$N_2O + OH \Leftrightarrow N_2 + HO_2$ (#8)

The main initiating reactions for NNH intermediate mechanism are

$NNH \Leftrightarrow N_2 + H$ (#9)

$NNH + M \Leftrightarrow N_2 + H + M$ (#10)

$NNH + O_2 \Leftrightarrow HO_2 + N_2$ (#11)

$NNH + O \Leftrightarrow OH + N_2$ (#12)

$NNH + H \Leftrightarrow H_2 + N_2$ (#13)

$NNH + OH \Leftrightarrow H_2O + N_2$ (#14)

There are some additional reactions associated with these mechanisms which also involve the conversion of N_2. These are removed together with the main initiating reactions.

Various triple flames were simulated by varying Φ_R, Φ_L, v_R, and v_L for each fuel at a global strain rate of $150s^{-1}$ and a global equivalence ratio of Φ=1.1. In order to specify conditions for a given flame, we first select Φ_R and Φ_L values, and then determine v_R and v_L using Eq. (1) and the following relation for the global Φ

$$v_R \chi_{F,R} + v_L \chi_{F,L} = \left(v_R \chi_{O,R} + v_L \chi_{O,L} \right) \Phi \nu \quad (2)$$

Here ν is the stoichiometric fuel/oxygen ratio, $\chi_{F,R}$ and $\chi_{F,L}$ the fuel mole fractions in rich and lean mixtures, respectively, and $\chi_{O,R}$ and $\chi_{O,L}$ the oxygen mole fractions in rich and lean mixtures, respectively. Table 1 lists the conditions for the four n-heptane and 1-heptene triple flames simulated in this study. The effect of strain rate on NO_x and PAH formation was examined by simulating Flames A1 and B1 at strain rates of $150s^{-1}$, $250s^{-1}$ and $500s^{-1}$.

Table 1: Conditions with Respect to Equivalence Ratio and Velocity of the Rich and Lean Fuel Streams for the Various Triple Flames Simulated.

Flame	Fuel	Φ_R	Φ_L	v_R(cm/s)	v_L(cm/s)
A1	n-heptane	1.5	0.8	85.7	63.3
B1	1-heptene	1.5	0.8	85.7	63.3
A2	n-heptane	2.0	0.5	88.3	59.7
B2	1-heptene	2.0	0.5	88.3	59.8
A3	n-heptane	2.5	0.4	97.6	50.2
B3	1-heptene	2.5	0.4	97.5	50.2
A4	n-heptane	3.0	0.35	104.6	43.0
B4	1-heptene	3.0	0.35	104.5	43.0

For the last part, triple flames of methyl decanoate, methyl-2-decenoate, and methyl-9-decenoate are simulated under the same conditions with Flame A1 and B1. The mechanism used is reduced mechanism for biodiesel surrogates, including methyl decanoate, methyl decenoate, and n-heptane, and consists of 115 species and 460 reactions. It is developed by Luo et al.[42] from University of Connecticut, Argone National Laboratory, and Lawrence Livermore National Laboratory, based on a detailed mechanism

developed by Lawrence Livermore National Laboratory. It has been validated through engine simulations. In our study, GRI 3.0 mechanism is combined into the original reduced mechanism to include NO chemistry. Although the original reduced mechanism doesn't include atomic C and $CH_2(S)$, which is included in GRI 3.0 mechanism, it does not much affect overall prompt NO production because contributions of these two species are usually small. Note that Chemkin 10101 is used for the simulations for this part.

3. Results and Discussion

3.1 Triple Flame Profiles of N-heptane and 1-Heptene

Figure 2 and Figure 3 present the temperature and NO profiles for the two n-heptane and 1-heptene triple flames simulated at conditions corresponding to A1, B1, A2, and B2 flames in Table 1. The n-heptane and 1-heptene flames exhibit similar global structure. For both fuels, the flame is characterized by the existence of a lean premixed (LP) reaction zone located on the left of the stagnation plane, a rich premixed (RP) reaction on the right of the stagnation plane, and a nonpremixed (NP) reaction zone near the stagnation plane. The peak temperature occurs in the nonpremixed zone, and is slightly higher (ΔT_{max}<50K) in 1-heptene flames compared to that in n-heptane flames. This can be attributed to the higher enthalpy of formation [43] and therefore higher adiabatic flame temperature for 1-heptene. In addition, the profiles in Figure 2 and Figure 3 indicate that as the level of partial premixing is reduced by simultaneously increasing Φ_R and lowering Φ_L (i.e., Flames A2 and B2), both the LP and RP zones move closer to the stagnation plane. This is due to the reduction in flame speeds associated with the LP and RP reactions zones. The comparison of NO profiles indicates notable differences in NOx emissions from the n-heptane and 1-heptene flames. The amount of NO formed in each of the three reaction zones is higher in 1-heptene flames compared to that in n-heptane flames. Moreover, as discussed next, the relative contributions of various NO formation routes are different in the three reaction zones.

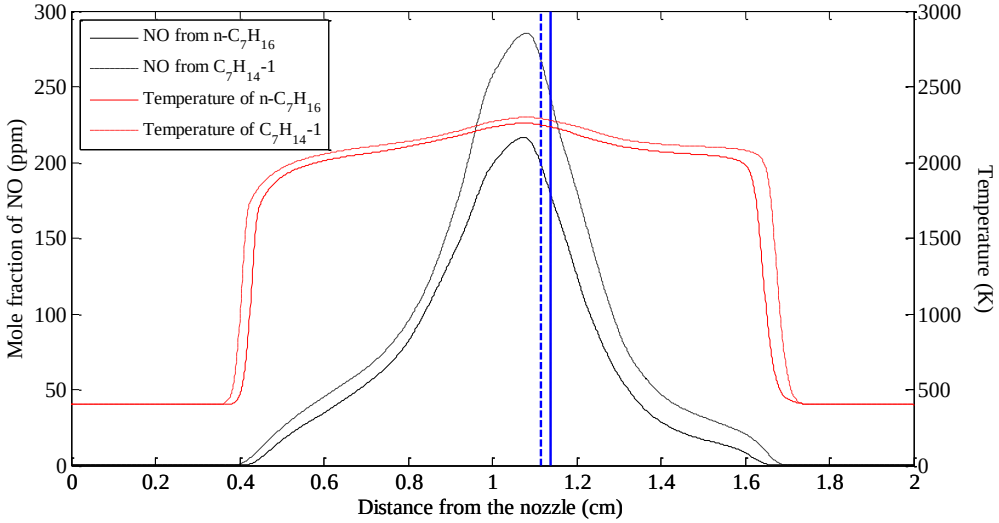

Figure 2: NO and temperature and profiles in n-heptane (A1) and 1-heptene (B1) flames established at Φ_R=1.5, Φ_L=0.8. Solid and dashed lines represent flames A1 and B1, respectively. Vertical lines represent the stagnation plane.

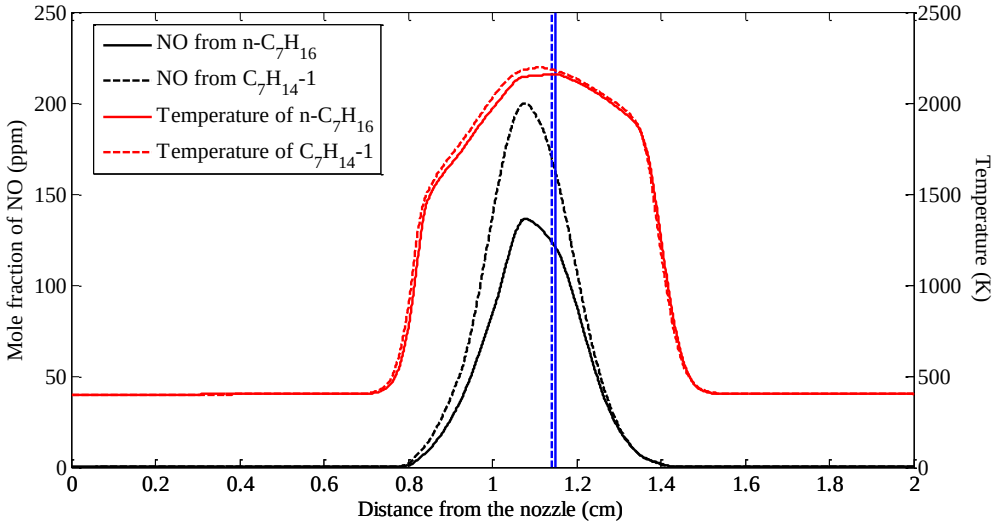

Figure 3: NO and temperature profiles in n-heptane (A2) and 1-heptene (B2) flames established at Φ_R=2.0, Φ_L=0.5. Solid and dashed lines represent flames A1 and B1, respectively. Vertical lines represent the stagnation plane.

3.2 Contributions of Various NO Formation Routes

Figure 4 and Figure 5 compare the relative NO contributions from the prompt, thermal, N_2O, and NNH mechanisms for the two n-heptane and 1-heptene flames discussed above. For these flames, the thermal mechanism appears to be the dominant source of NO, although contributions from the other three mechanisms are also significant. Moreover, the relative contributions of various mechanisms are different in each reaction zone. While NO formation in the RP zone is primarily due to the prompt route, that in the NP zone is dominated by the thermal route. In contrast, NO in the LP zone is formed mainly through the NNH and N_2O routes, with some additional contribution from the thermal route. This is shown more clearly in Figure 6, which plots the rate of production of total NO as well as of prompt, thermal, N_2O intermediate, NNH intermediate NO in Flames A1 and B1. As indicated in this figure, Thermal NO has the highest production rate in the NP reaction zone where the temperature is the highest. However, the thermal NO production rate is also significant in the LP zone as well as in the region between the LP and NP reaction zones. This is due to the abundance of O radical in the LP zone, and the transport of heat from the NP zone to the LP zone. In contrast, the thermal NO production rate is negligible in the RP zone, although temperature in this zone is relatively high. This is because of the low concentrations of O and OH in this zone, as these species react with N_2 and N through reactions $O + N_2 \rightarrow NO + N$, $N + O_2 \rightarrow NO + O$, and $N + OH \rightarrow NO + O$ to form thermal NO.

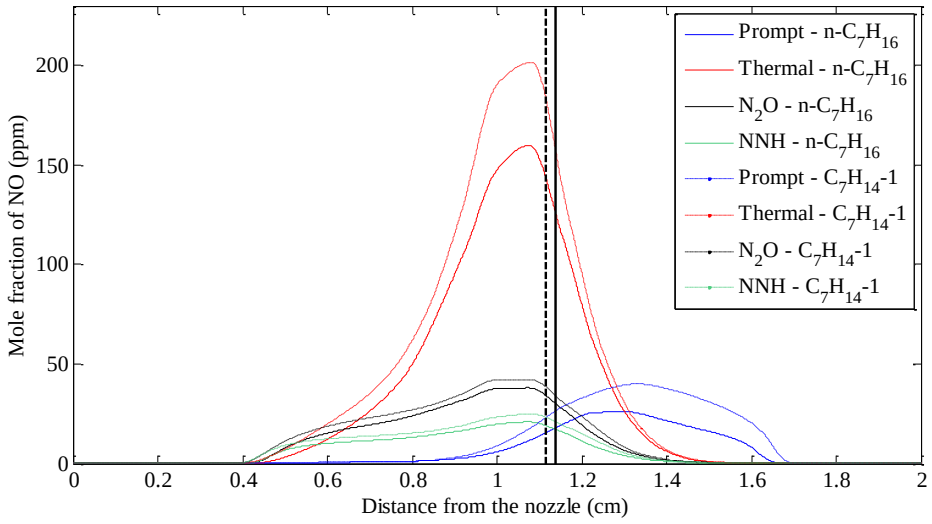

Figure 4: NO profiles corresponding to the thermal, prompt, N_2O intermediate, and NNH mechanisms for n-heptane (A1) and 1-heptene (B1) flames. Solid and dashed lines represent flames A1 and B1, respectively. Vertical lines represent the stagnation plane.

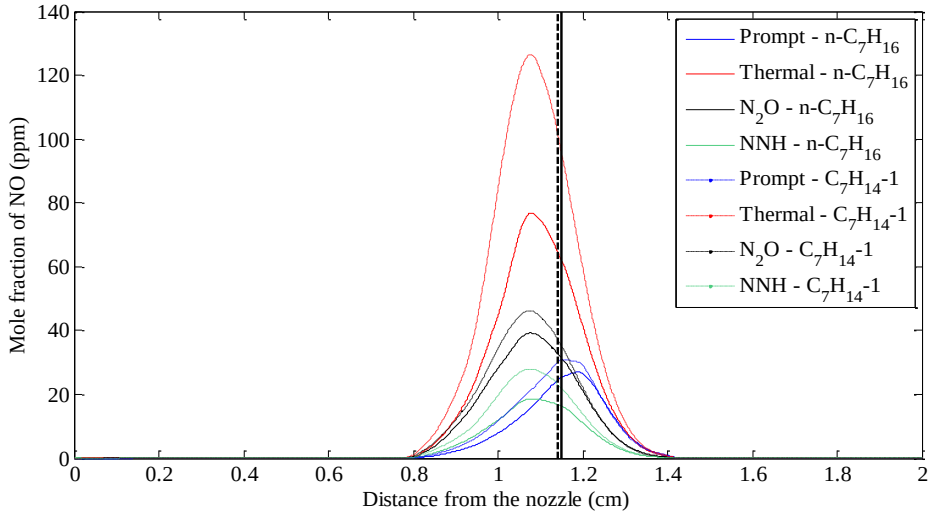

Figure 5: NO profiles corresponding to the thermal, prompt, N_2O intermediate, and NNH mechanisms for n-heptane (A2) and 1-heptene (B2) flames. Solid and dashed lines represent flames A1 and B1, respectively. Vertical lines represent the stagnation plane.

Figure 6 further indicates that most of the prompt NO is produced in the RP zone, due to the abundant hydrocarbon radicals in this region. As shown in Figure 7, the C_2H_2 and CH concentrations are the highest in this region, where the prompt NO is formed through the reaction of CH with N_2. Also note that both the peak prompt NO production rate and the peak CH concentration are located near x=1.6 cm from the fuel-lean nozzle. In addition, as indicated in Figure 6, NO formation in the lean premixed reaction zone occurs mainly through the NNH and N_2O routes. In fact the NNH concentration is higher in the RP zone than that in the LP zone, as shown in Figure 8. However, O radicals are more abundant in the LP zone and can support the key reaction $NNH + O \rightarrow NH + NO$. In contrast, the N_2O concentration is significantly higher in the LP zone, where N_2O is formed through $N_2 + O + M \rightarrow N_2O + M$. Moreover, since these reactions are not directly related to hydrocarbon species (C_2H_2 and CH), the slightly higher NO formed through the NNH and N_2O routes in the LP zone of 1-heptene flame compared to n-heptane flame may be due to the higher temperature of 1-heptene flame.

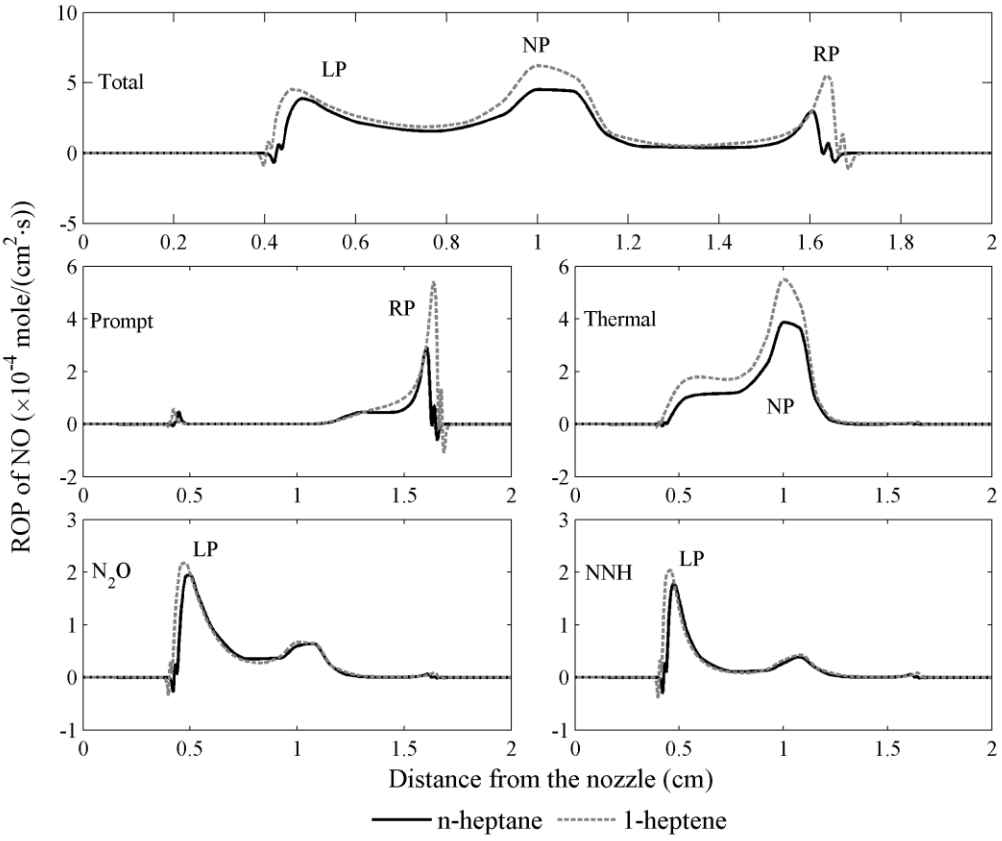

Figure 6: Rate of production of total NO as well as of prompt, thermal, N_2O intermediate, NNH intermediate NO in Flames A1 and B1.

Another important observation from Figure 6 is the higher prompt NO in 1-heptene flame (B1) compared to that in n-heptane flame (A1). This is largely due to the higher concentrations of C_2H_2 and CH in the rich premixed region of 1-heptene flame, as indicated in Figure 7. Moreover, the higher total NO formed in 1-heptene flame than in n-heptane flame is mainly due to the thermal and prompt contributions; the NNH and N_2O contributions are nearly the same in the two flames. The higher thermal NO formed in 1-heptene flame is due to the higher temperature in this flame, while the higher prompt NO in 1-heptene flame is due to higher CH concentration. Further discussion on the effect of fuel molecular structure on NO_x formation is provided in a later section.

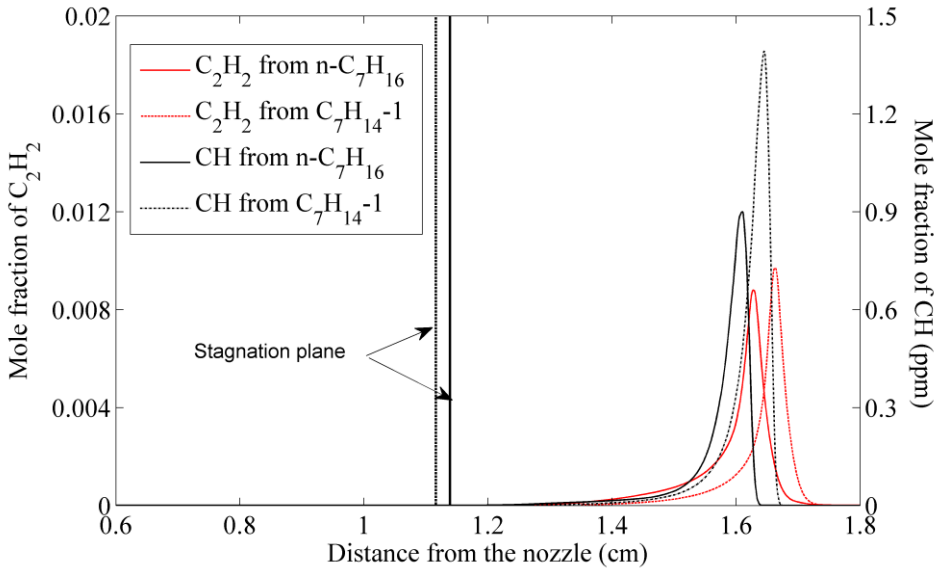

Figure 7: C_2H_2 and CH profiles in Flames A1 and B1. Vertical lines represent the stagnation plane.

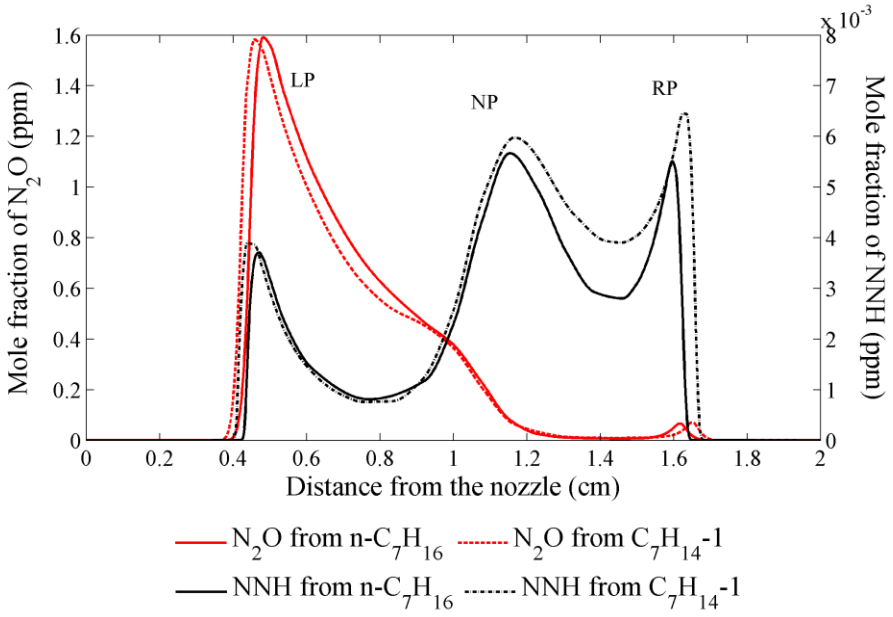

Figure 8: N_2O and NNH profiles in Flames A1 and B1.

The relative contributions of the various NO formation routes in each reaction zone of a triple flame depend strongly on the level of premixing or stoichiometries of the fuel-lean and fuel-rich mixtures. This can be seen clearly from the comparison of NO contributions from the prompt, thermal, N_2O, and NNH mechanisms in Flames A2 and B2 (Φ_R =2.0 and Φ_L =0.5) shown in Figure 9, and in Flames A1 and B1 (Φ_R =1.5 and Φ_L =0.8), shown in Figure 6. In Flames A2 and B2, the LP and RP zones, which are located at 0.8cm and 1.4cm from the fuel-lean nozzle (cf. Figure 3), are relatively weak compared to the NP reaction zone. Consequently, as indicated in Figure 6 and Figure 9, most of the NO through the thermal, N_2O, and NNH routes is formed near this reaction zone, while the prompt NO is formed in the region between the RP and NP reaction zones. These aspects are further discussed in the next section.

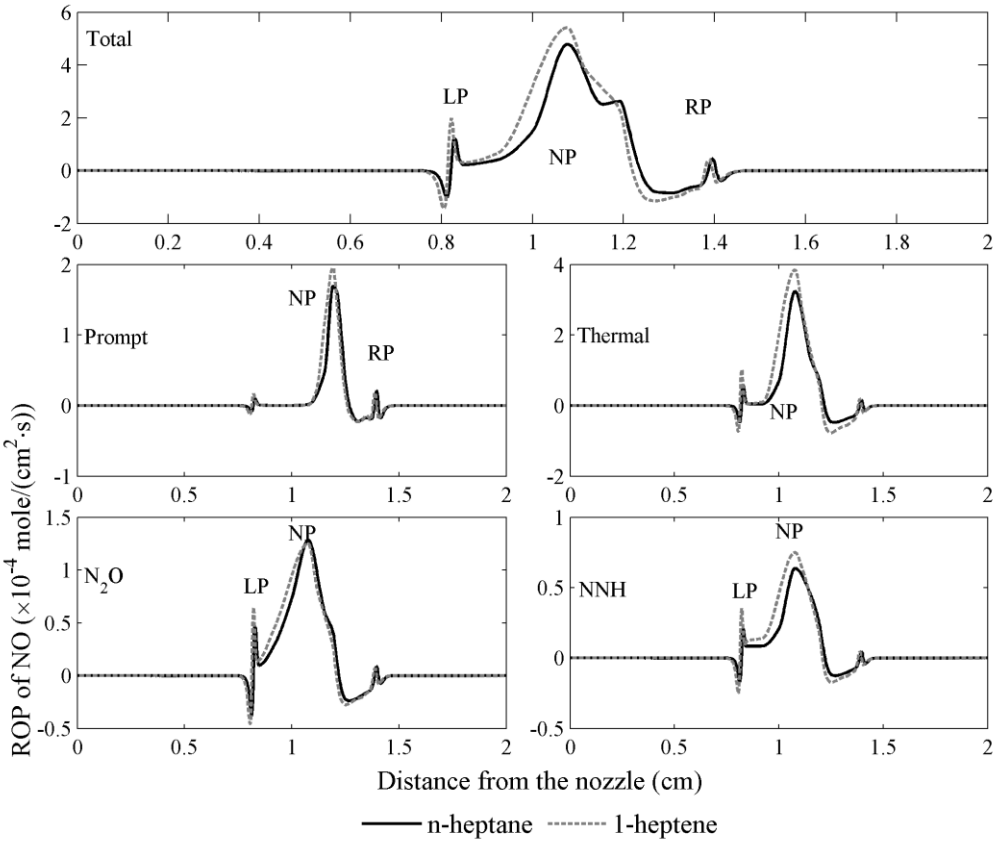

Figure 9: Rate of production of total NO and of prompt, thermal, N_2O intermediate, NNH intermediate NO in Flames A2 and B2.

3.3 Effect of the Double Bond

Some insight regarding the effect of fuel molecular structure on prompt NO formation can be gained from the C_2H_2 and CH profiles presented in Figure 10 for Flames A2 and B2. While the C_2H_2 profile contains one peak in the RP zone, the CH profile shows two peaks, one in the RP zone and the other in region between the RP and NP zones. The second peak is due to the incomplete conversion of C_2H_2 to CH in the rich premixed zone. Note that the CH peak in the rich premixed zone is significantly higher in 1-heptene flame than in n-heptane flame, while the second peak shows very little difference between the two fuels. Between these two peaks, the reactions producing CH slow down due to the very low concentrations of O and H radicals there. The chemistries that dominate the regions of the two peaks of CH are different. In the RP zone, the decomposition of the original fuel molecule into smaller species plays an important role. 1-heptene produces more C_2H_2 and thus more CH in the first peak compared to n-heptane. This is consistent with the fact that the first peak of CH is formed right after the peak of C_2H_2. However, the conversion of C_2H_2 to CH is only partially completed. Consequently, a second peak is formed downstream of the first peak. However, the effect of the double bond chemistry of 1-heptene is diminished in this region, since the large hydrocarbon molecules are already broken down in the rich premixed zone. Since most of the prompt NO is produced in the region between the two reaction zones and not in the rich premixed zone, the effect of the double bond fuel on prompt NO formation is reduced for this flame.

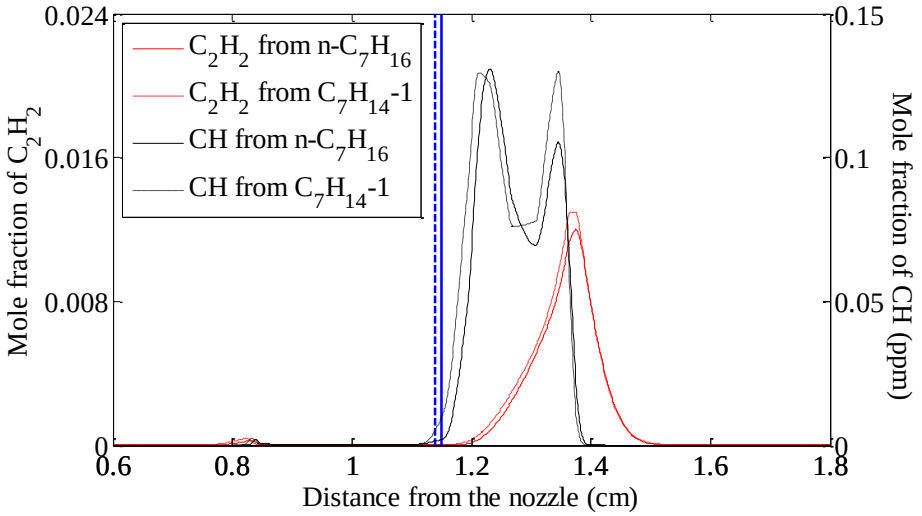

Figure 10: C_2H_2 and CH profiles in Flames A2 and B2. Vertical lines represent the stagnation plane.

3.4 Effect of Partial Premixing and Strain Rate on NOx Emission Index

Figure 11 plots the emission index of total NO (EINO) and of the prompt, thermal, N_2O, and NNH mechanisms for the four n-heptane and 1-heptene triple flames. All these flames are simulated at a global strain rate of a_g=150s^{-1} and global equivalence ratio of Φ=1.1. Results concerning the effect of stain rate on the triple flame structure and NOx emission are shown in Figure 13 and Figure 12. The emission index of NO is defined as

$$EINO = \frac{\int_0^L MW_{NO}\dot{\omega}_{NO}dx}{-\int_0^L MW_{fuel}\dot{\omega}_{fuel}dx}$$

There are several observations from Figure 10. First, 1-heptene flames have higher EINO than n-heptane flames for all the four cases. The EINO values for the thermal, prompt, and NNH mechanisms are also higher for 1-heptene compared to n-heptane, while those for the N_2O mechanism are essentially the same

for the two fuels. Second, as the level of premixing is reduced (going from left to right), the total EINO decreases for both the fuels. The difference in EINO between the two fuels also decreases as the level of premixing is reduced. However, the relative contributions of various NO routes to total EINO exhibit a more complex behavior. As the level of premixing is reduced, the contribution of thermal EINO decreases significantly, while those of prompt and NNH increase, and that of N_2O remains about the same. It is also important to note that the variation of prompt EINO with the level of premixing correlates with the peak CH mole fraction.

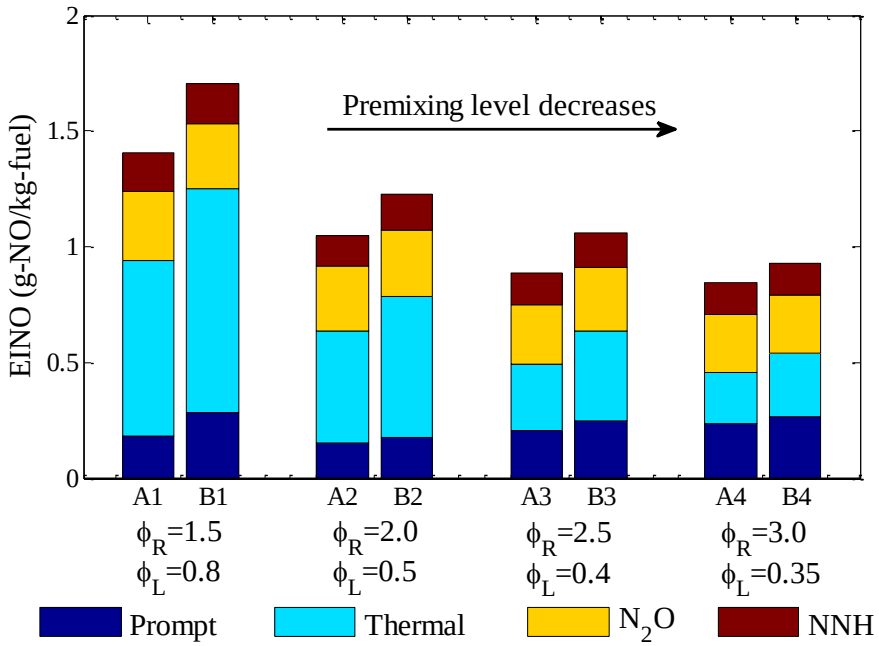

Figure 11: Emission index for the total NO and for the prompt, thermal, N_2O, and NNH mechanisms for the four n-heptane and 1-heptene triple flames, all at a global strain rate of a_g=150s^{-1} and global equivalence ratio of Φ=1.1. Each two neighboring bars represent n-heptane (left) and 1-heptene (right) flames, respectively, at the same conditions. The level of premixing for the four flames decreases going from left to right along the "Flame number" axis. Φ_L and Φ_R values for these flames are given in Table 1.

Figure 13 presents the temperature profiles for n-heptane and 1-heptene triple flames established at strain rates of 150s^{-1}, 250s^{-1}, and 500s^{-1}, and ϕ_L=0.8, ϕ_R=1.5. As the strain rate is increased, the peak flame

temperature, which occurs in the NP zone, first increases slightly and then decreases. This is due to the competing effects of reduced residence time at higher strain rates, and enhanced interaction between the NP zone and the two premixed zones. As discussed by Guo et al.[44], as the strain rate is increased, the physical separation between the reaction zones is reduced (cf. Figure 13), which leads to enhanced interaction between the NP and two premixed reaction zones. The effect of strain rate on NO formation is depicted in Figure 12, which plots the emission index of total NO and of prompt, thermal, N_2O, and NNH mechanisms for the n-heptane and 1-heptene triple flames at different strain rates. An important observation is the higher NO emission in 1-heptene flames compared to that in n-heptane flames irrespective of the strain rate. Moreover, as strain rate is increased, the EINO first increases and then decreases, consistent with the variation of peak flame temperature with strain rate. The EINO values for the prompt, thermal, N_2O, and NNH mechanisms also follow a similar trend. However, the relative contribution of prompt NO becomes more pronounced at higher strain rates, while that of thermal NO is reduced to the reduced residence time.

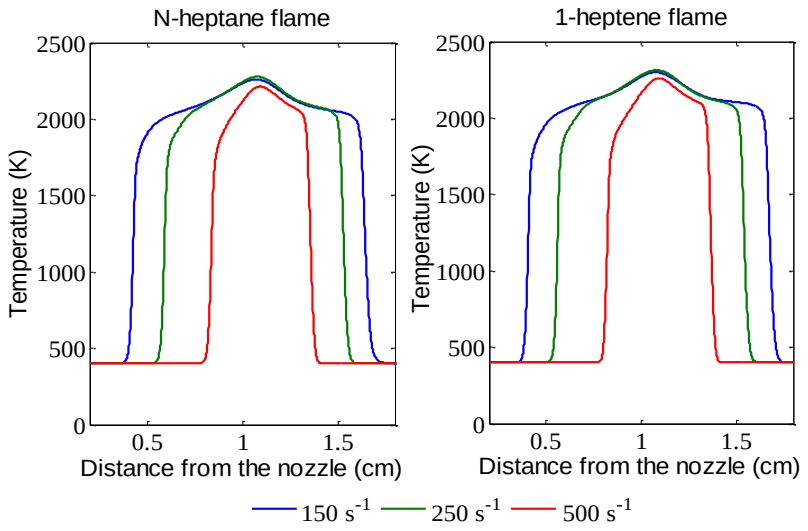

Figure 12: Temperature profiles for n-heptane and 1-heptene triple flames at different strain rates, and ϕ_L=0.8 and ϕ_R=1.5.

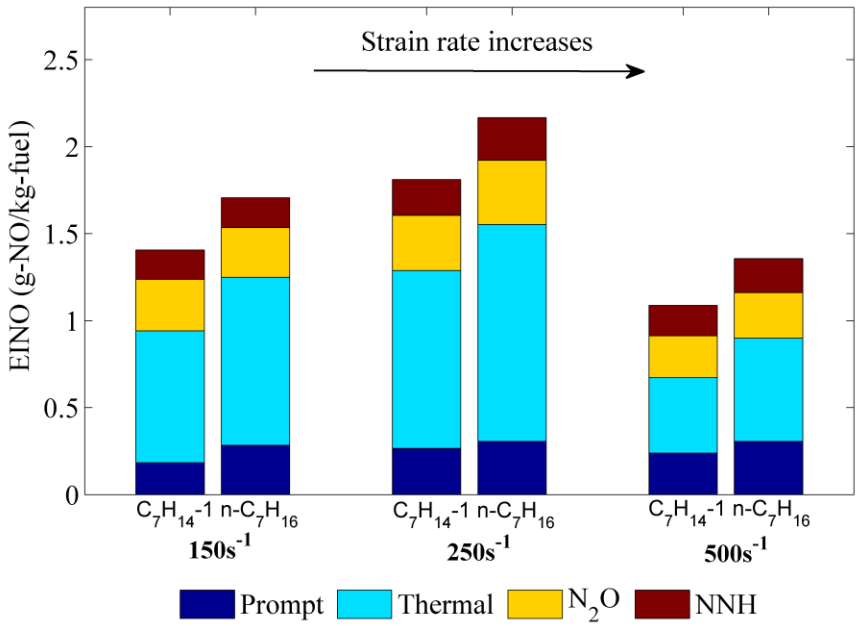

Figure 13: Emission index for the total NO and for the prompt, thermal, N_2O, and NNH mechanisms for the four n-heptane and 1-heptene triple flames at global strain rates of a_g=150s^{-1}, 250s^{-1}, and 500s^{-1}, and for ϕ_L=0.8 and ϕ_R=1.5.

3.5 Effect of Double Bond, Premixing, and Strain Rate on PAH Formation

The effect of unsaturated bond on soot emissions is examined in terms of the benzene profiles in n-heptane and 1-heptene triple flames. The capability of the simulation model for predicting benzene and larger PAH species, including naphthalene ($C_{10}H_8$), phenanthrene ($C_{14}H_{10}$) and pyrene ($C_{16}H_{10}$), has been demonstrated in our previous study[14]. Moreover, the cited study has shown a direct correlation between the amounts of benzene and larger PAH species. Figure 14 and Figure 15 present benzene profiles for the various n-heptane and 1-heptene triple flames established at different levels of premixing and strain rates. An important observation from these figures is the significantly higher benzene formation in 1-heptene flames compared to that in n-heptane flames. As discussed later, this can be attributed to the effect of double bond on the 1-heptene pyrolysis chemistry, leading to the increased formation of allyl radical

(C_3H_5), 1,3-butadiene (C_4H_6), propargyl (C_3H_3), and other precursors, and thus significantly higher benzene formation in 1-heptene flames. It is also important to note that most of benzene is formed in the RP zone, which is characterized by high concentrations of intermediate hydrocarbons, such as C_3H_5, C_4H_6, and C_3H_3. Regarding the effect of strain rate, results indicate that the amount of PAH formed in 1-heptene flames is consistently higher than that in n-heptane flames irrespective of the strain rate. However, larger PAH species is more sensitive to strain rate than small ones, which is also found in acetylene counter-flow diffusion flames by Yamanoto et al[45]. Figure 16 shows the change of pyrene ($C_{16}H_{10}$) and benzene formation after strain rate increased from 150s^{-1} to 500s^{-1}.

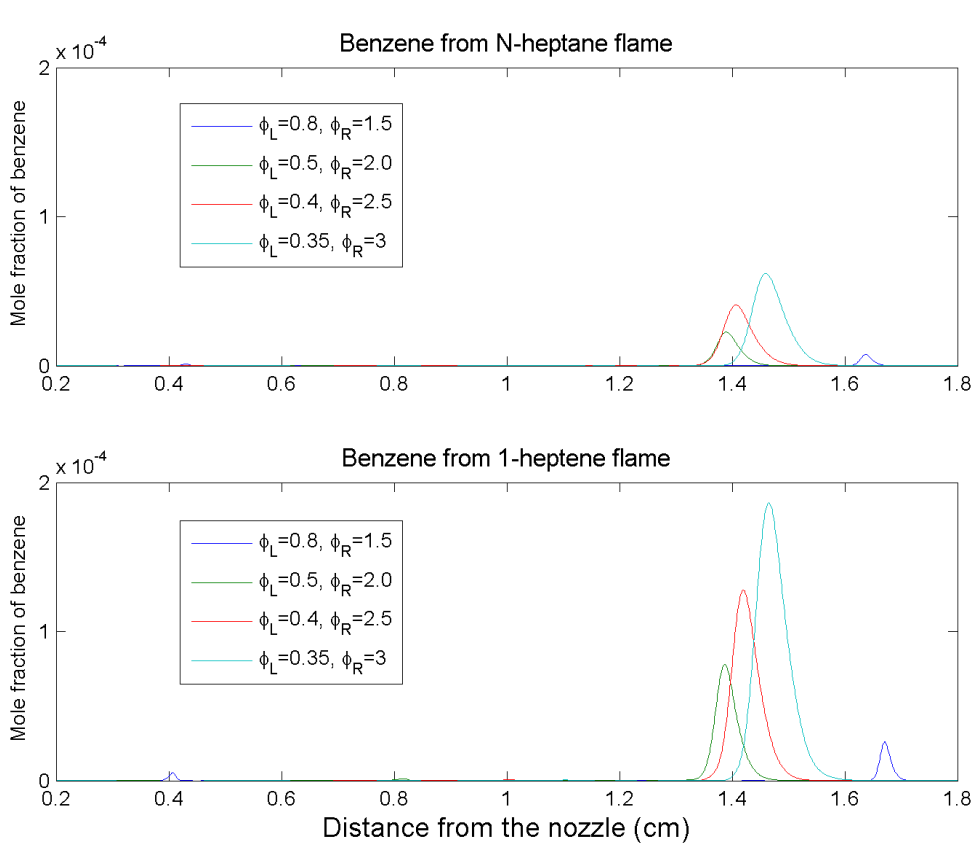

Figure 14: Benzene profiles in n-heptane and 1-heptene flames established at different levels of partial premixing. Strain rate is 150 s^{-1}.

In order to gain further insight into the effect of double bond on PAH formation, a reaction pathway analysis was performed, and results are summarized in Figure 16, which present the dominant pathways for the formation of benzene in 1-heptene and n-heptane flames, respectively, at ϕ_L=0.8, ϕ_R=1.5 and strain rate of 150s^{-1}. The pathway analysis shows general consistency with previous studies by Hongzhi Zhang et al.[46,47,48] on n-heptane decomposition, including the reactions involving olefins formed in such process. In the following discussion, we'll describe the reaction pathway along with the relative importance of different routes in deciding the overall benzene formation regarding our cases, in which the high temperature pyrolysis of the fuels are of great significance in such formation.

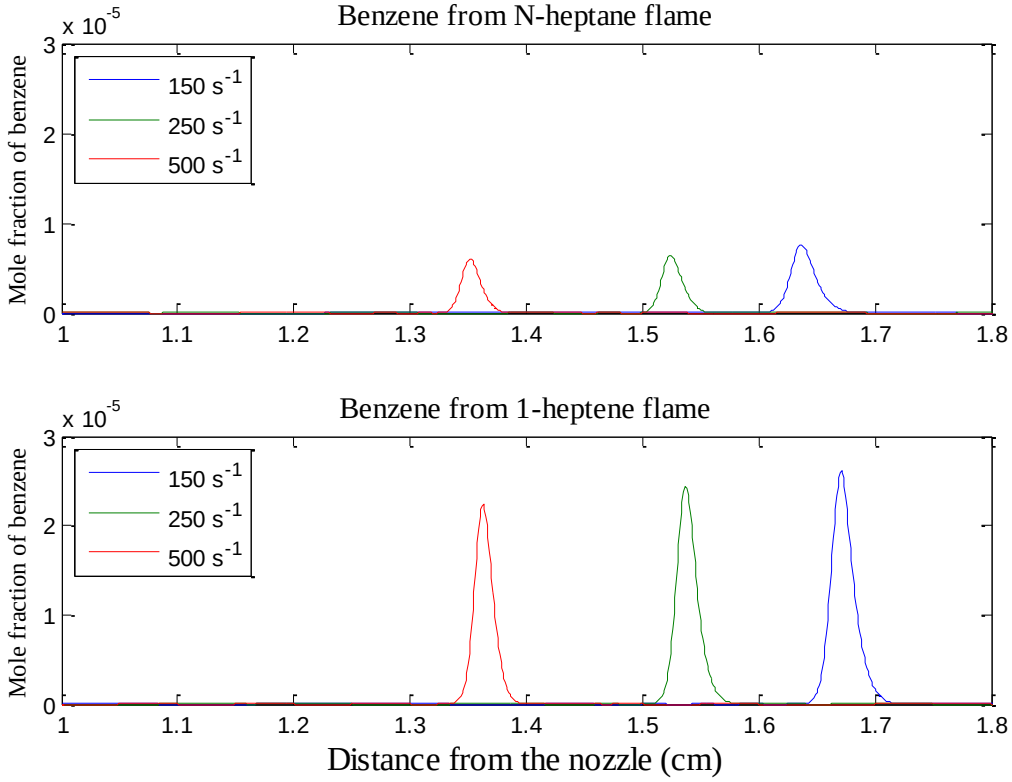

Figure 15: Benzene profiles in n-heptane and 1-heptene flames established at different strain rates, and ϕ_L=0.8 and ϕ_R=1.5.

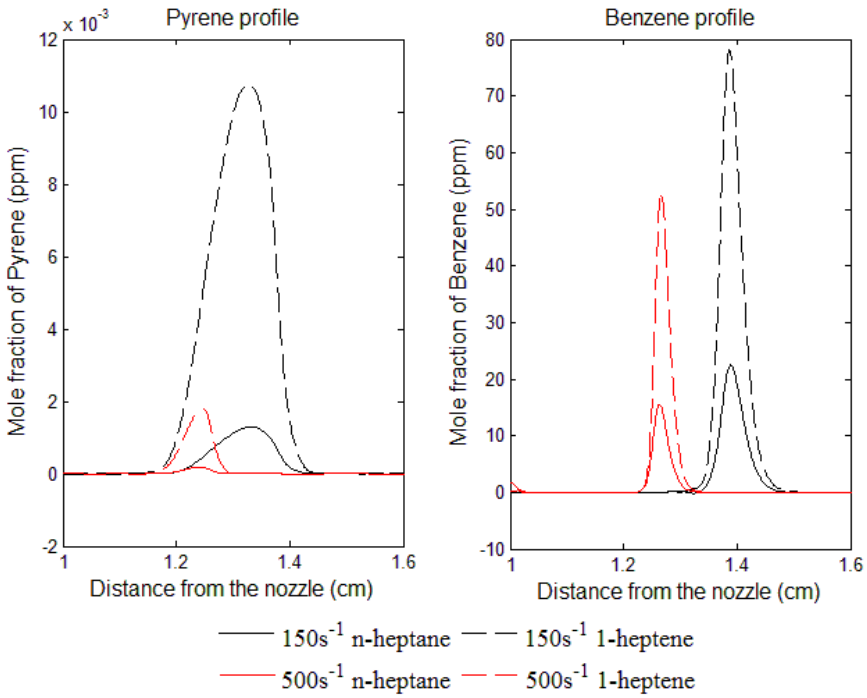

Figure 16: Strain rate effect on benzene and pyrene concentrations in n-heptane and 1-heptene flames.

While the oxidation of these two fuels follows different paths depending upon the temperature, benzene is mainly formed through the recombination reaction of propargyl radicals (C_3H_3)[49]. Most of C_3H_3 is formed from allyl radicals (C_3H_5), and the formation of allyl from fuel decomposition is quite different for 1-heptene and n-heptane fuels, as can be seen on the left side of Figure 17 (a) and (b). At high temperatures (>1200K), typical of flame environment, most of 1-heptene directly decomposes into C_3H_5 and C_4H_9. In contrast, the decomposition of n-heptane at high temperature does not form C_3H_5 directly. Instead, it forms various alkyl radicals, such as CH_3, C_6H_{13}, C_2H_5, C_5H_{11}, C_3H_7 and C_4H_9, most of which then decompose into C_2H_4 and CH_3 (not shown) through β scission and H abstraction reactions. Similarly, the butyl (C_4H_9) formed from 1-heptene also decomposes into C_2H_4. In fact, this is the main source of ethylene in 1-heptene flame (cf. Fig.17a), while there are multiple alkyl species (C_6H_{13}, C_5H_{11}, C_4H_9, C_3H_7, etc.) that form ethylene in n-heptane flame (cf. Fig. 17b). Consequently, the ethylene concentration

is higher in n-heptane flame compared to that in 1-heptene flame, as indicated in Fig. 18. Ethylene subsequently forms vinyl (C_2H_3), which can also produce benzene through its reaction with butadiene. However, the higher C_2H_4 concentration does not imply increased benzene production in n-heptane flame, since the butadiene concentration is much lower in this flame compared to that in 1-heptene flame, as shown in Fig. 18. This aspect is further discussed in the following.

As indicated in Fig. 18, the low-temperature (<1200K) oxidation paths of n-alkane and 1-alkene are also significantly different. The decomposition of n-heptane is initiated by H abstraction forming n-alkyl radicals, which then break into various 1-alkenes (C_3H_6, C_4H_8, C_5H_{10}) and smaller alkyls (CH_3, to C_5H_{11}) through β-scission and H abstraction reactions. The smaller alkyls subsequently form C_2H_4, which lead to the production of benzene through vinyl (C_2H_3), similar to the high-temperature reaction path discussed above. The various 1-alkanes (except C_2H_4) on the other hand represent the main source of allyl and butadiene, which subsequently form benzene. However, the formation of allyl competes with that of butadiene in n-heptane flames, unlike the case for 1-heptene flames, in which the path to butadiene is preferred. Consequently, the amount of butadiene formed in n-heptane flames is significantly lower than that in 1-heptene flames (cf. Fig. 18), as stated earlier. The low-temperature oxidation of 1-heptene follows three different paths. The main path involves H abstraction at the alpha-carbon location near the double bond, forming 1-butylallyl radicals, which then break into 1,3-butadiene and propyl. The second path involves H addition and formation of n-C7 alkyl radicals, which then follow a similar path as that for n-heptane discussed above. The third path involves the decomposition of 1-heptene through H abstraction from other C-H bonds, forming 1-C_7H_{13} radicals, which then form propargyl (though allyl) and 1-C_4H_7, and subsequently benzene. In summary, for the low-temperature reaction path, n-heptane tends to produce more allyl than 1-heptene. However, in the rich premixed flame environment, the benzene formation is dominated by the high-temperature reaction path, with the implication that significantly higher amount of benzene is formed in 1-heptene flames compared to that in n-heptane flames.

Finally, it should be mentioned that C_2H_2 is known to be important precursor for PAH and soot production. As stated earlier, the presence of double bond leads to the higher production of C_2H_2 in 1-heptene flames than in n-heptane flames. In the context of Fig. 16, C_2H_2 is mainly formed from vinyl, and produces benzene through its reaction with C_4H_5 radicals, which are formed from butadiene. Acetylene subsequently plays an important role in the formation of larger PAH species through the HACA (hydrogen abstraction acetylene addition) mechanism. It is also important to note that while the concentration of C_2H_4 is higher in n-heptane flames, that of C_2H_2 is higher in 1-heptene flames. This is due to the fact that C_2H_2 is produced from both C_2H_4 (through vinyl) and C_4H_5 (which produces C_2H_2 and C_2H_3), and the concentration of C_4H_5 is noticeably higher in 1-heptene flames, leading to the increased production of C_2H_2 in these flames.

(a) 1-Heptene → benzene:

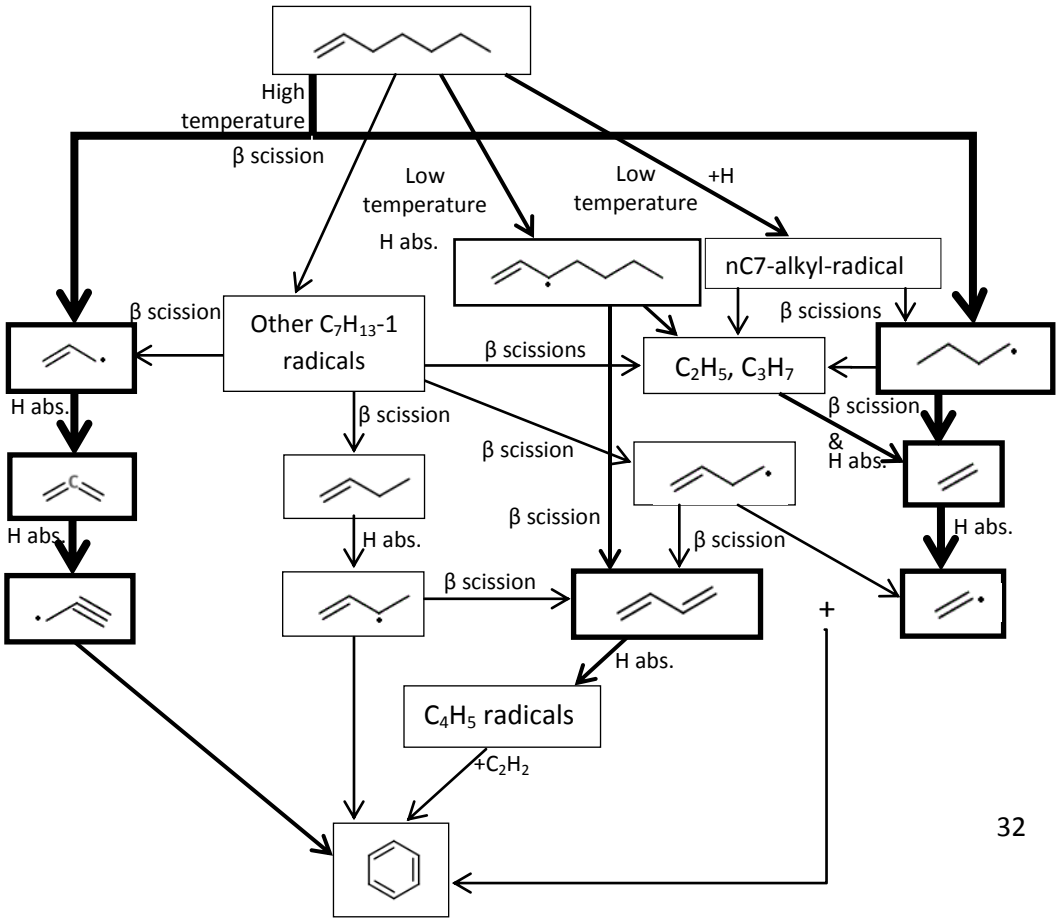

(b) n-Heptane → benzene:

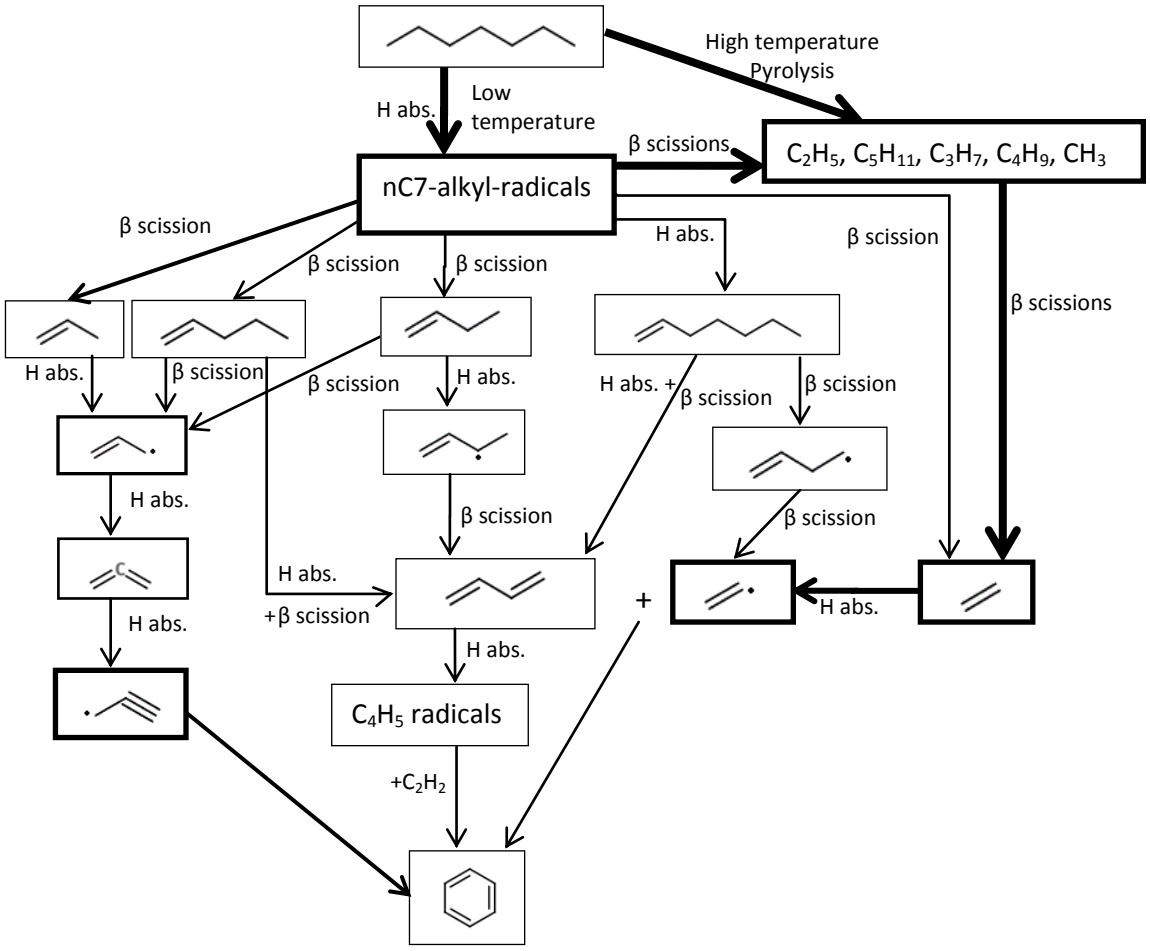

Figure 17: Benzene formation pathways in 1-heptene (a) and n-heptane (b) flames.

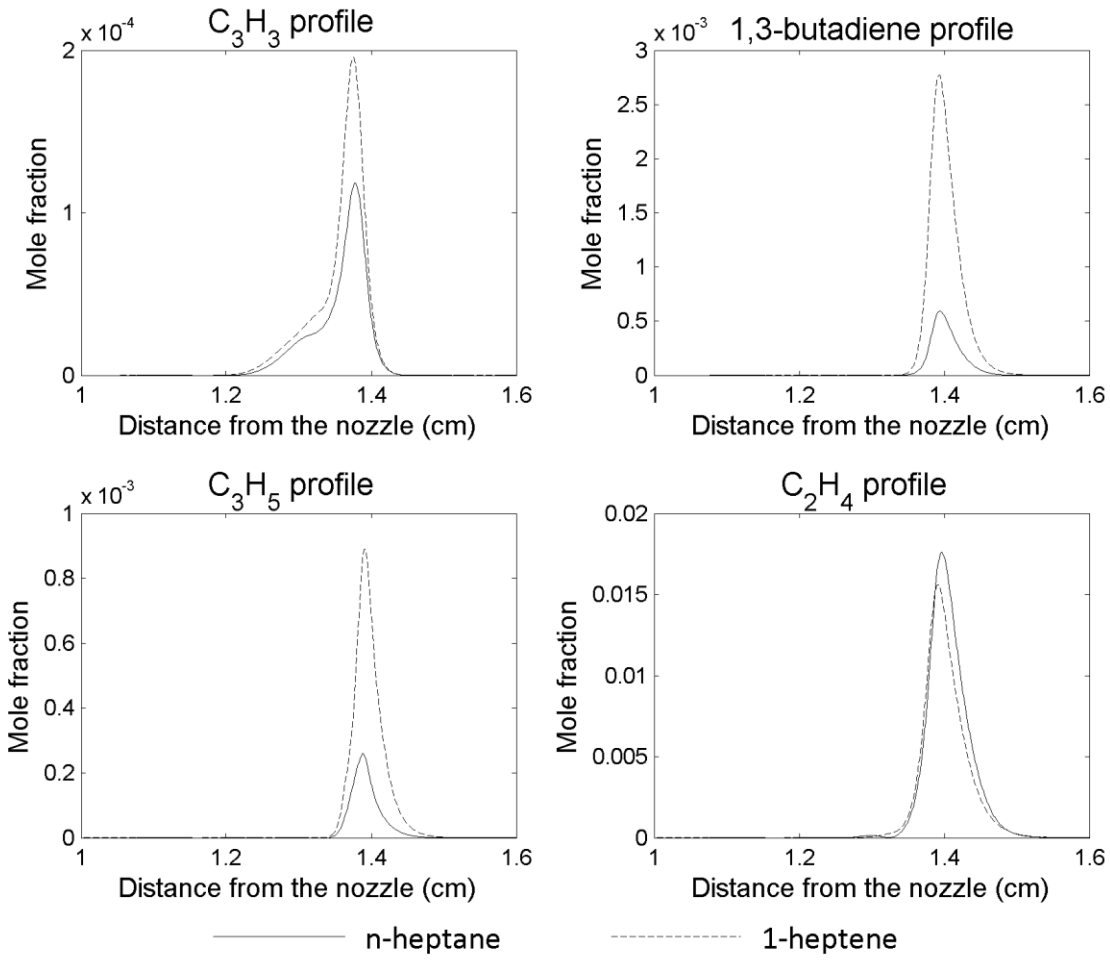

Figure 18: Concentration profiles of benzene precursors C_3H_3, C_3H_5, 1,3-butadiene, and C_2H_4 in n-heptane and 1-heptene flames.

Figure 19 presents the emission indices of benzene and naphthalene for the four n-heptane and 1-heptene triple flames discussed in the context of Figure 12. The effect of double bond is more significant on naphthalene formation than on benzene formation. As the level of premixing is reduced, the PAH emission indices increase for both the fuels, which is due to the increasingly higher amounts of intermediate hydrocarbons (C_3H_5, C_3H_3, and C_4H_6) formed and the lack of oxidizer in the RP zone. It can also be seen that the change of premixing level is more effective to naphthalene. This, together with the above discussions, shows that the effect of double bond, strain rate, and premixing level has greater effect on larger PAH species. In addition, results indicate that for all the four cases of premixing, the PAH

emission from 1-heptene flames is significantly higher than that from n-heptane flame. The level of premixing doesn't seem to effectively change the relative increase of benzene from 1-heptene over n-heptane. However, for the production of large PAH species, for example pyrene, which has four aromatic rings, premixing level does change the relative difference between the two fuels.

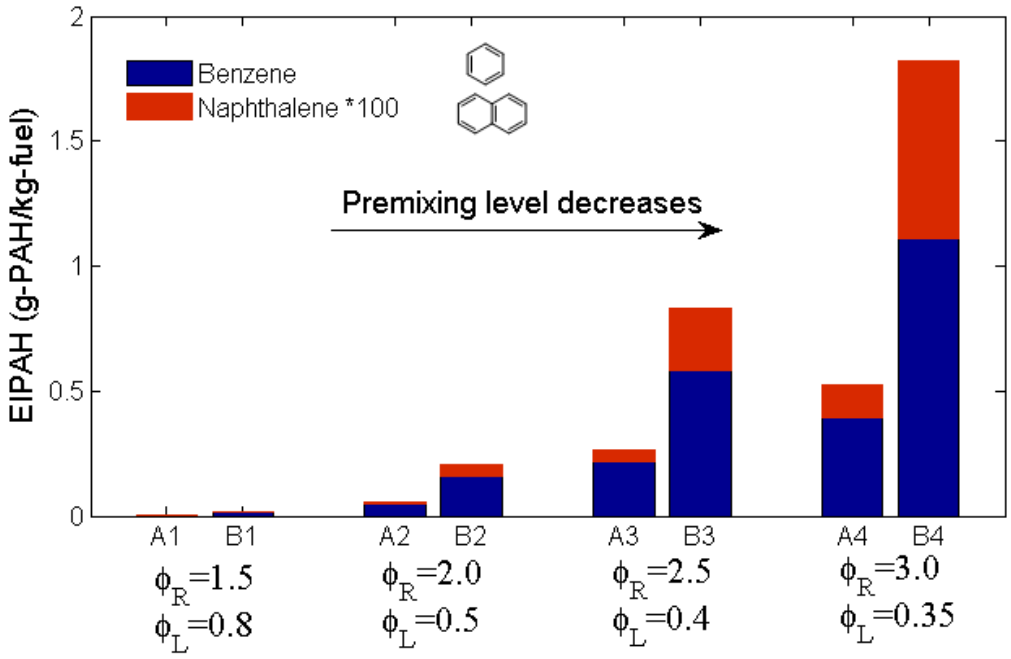

Figure 19: Emission index of benzene and naphthalene for the four n-heptane and 1-heptene triple flames, all at a global strain rate of a_g=150s^{-1} and global equivalence ratio of Φ=1.1. Each two neighboring bars represent n-heptane (left) and 1-heptene (right) flames, respectively, at the same conditions. The level of premixing for the four flames decreases from left to right along the "Flame number" axis. Φ_L and Φ_R values for these flames are given in Table 1.

3.6 Flames of Methyl Esters

In this part, as an extension to the heptane and heptene flames, an investigation on flames formed by methyl esters with and without unsaturation is presented. Simulations are conducted for triple flames of methyl decanoate, methyl-2-decenoate, and methyl-9-decenoate, under the same conditions with Flame A1 and B1 of C7 hydrocarbons, including the same strain rate ($150s^{-1}$) and equivalence ratios ($\mathbf{\Phi_L}$ =0.8 and $\mathbf{\Phi_R}$=1.5). For convenience, the molecular structures of the three fuels are shown in Figure 20.

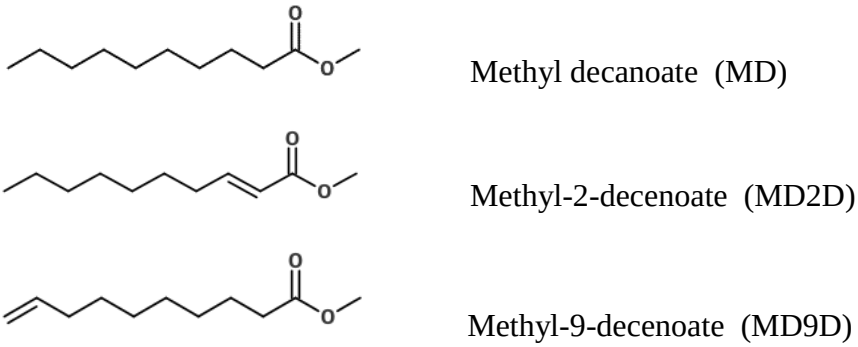

Figure 20: Molecular structure of methyl decanoate, methyl-2-decenoate, and methyl-9-decenoate

Methyl-9-decenoate (it will be called MD9D from now on) has its C=C bond farthest from the methyl ester group among its methyl decenoate isomers, while methyl-2-decenoate (it will be called MD2D from now on) has the closet one. This will influence the initiation reactions and consequently produce different intermediate species in combustion.

The result of the triple flame simulation is shown in Figure 21. As expected from previous studies by Garner et al.[9,10], the addition of methyl ester group on long alkane and alkene chains doesn't change the fact that the unsaturated C=C bond will increase formation of C_2H_2, CH and thus prompt NO. However, there is a large difference in CH profiles between MD2D and MD9D. MD2D flame has a higher production of NO than the one of MD9D, but a significantly lower production of CH in the rich premixed reaction zone, where the majority of CH and prompt NO is formed. Therefore, formation of prompt NO in

MD9D flame is the largest among the three fuels. The larger amount of NO in MD2D flame is contributed by thermal NO, due to a slightly higher flame temperature in this case.

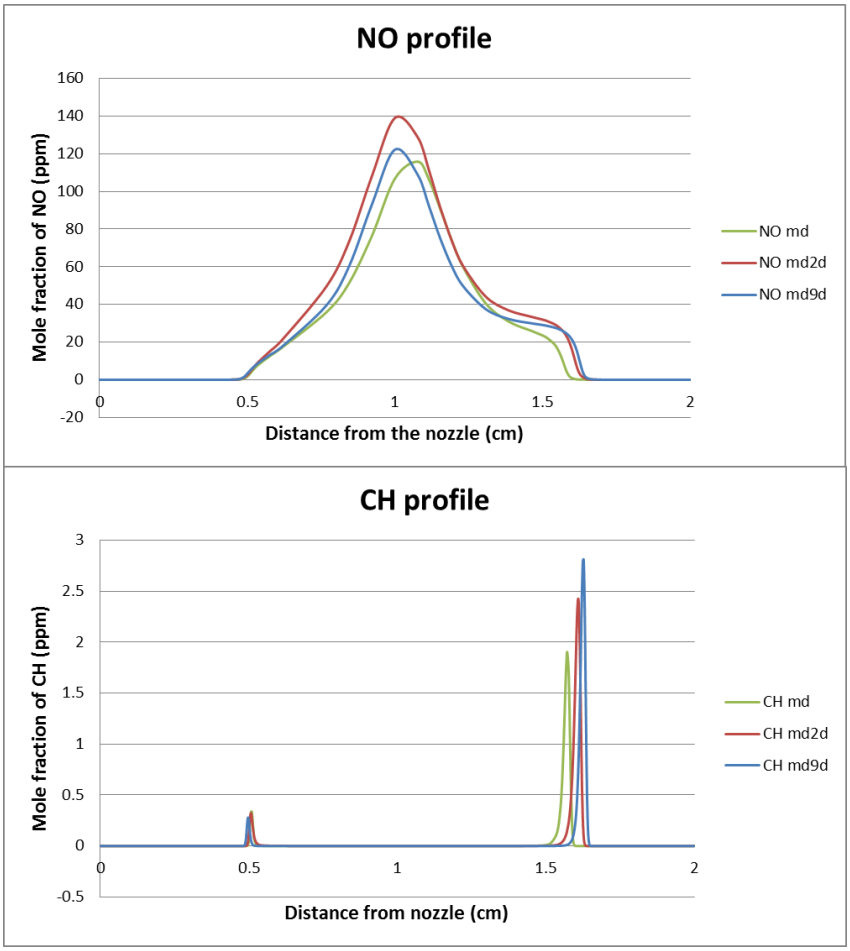

Figure 21: Comparison of NO and CH species profiles in a counter-flow triple flame formed by methyl decanoate (md), methyl-2-decenoate (md2d), and methyl-9-decenoate (md9d), respectively.

For better understanding, the three fuels are also compared in a diffusion flame with low strain rate ($12.5s^{-1}$). The result is shown in Figure 22. It again shows an increase of CH in MD9D flame, compared to that in MD2D flame. Thus, the difference in CH formation observed in these flames is probably due to the chemical kinetics of the decomposition of these two fuels. Due to the complexity of the combustion

chemistry of these two fuels, a detailed analysis is not done for the formation of methyl radical or acetylene. Moreover, the validity of this reduced model in predicting MD2D decomposition is not as reliable as MD9D and MD, because, as stated in the corresponding article[42], this reduced mechanism is aimed at simulating MD and MD9D combustion, although it contains MD2D. In particular, the reduced mechanism only contains the reactions of hydrogen addition on the alkenyl side chain for MD2D. Thus we are not able to compare the effect of position of the double bond using this reduced mechanism.

Above all, the fact that the unsaturated methyl ester fuels will produce more NO than their saturated counterparts remains unchanged.

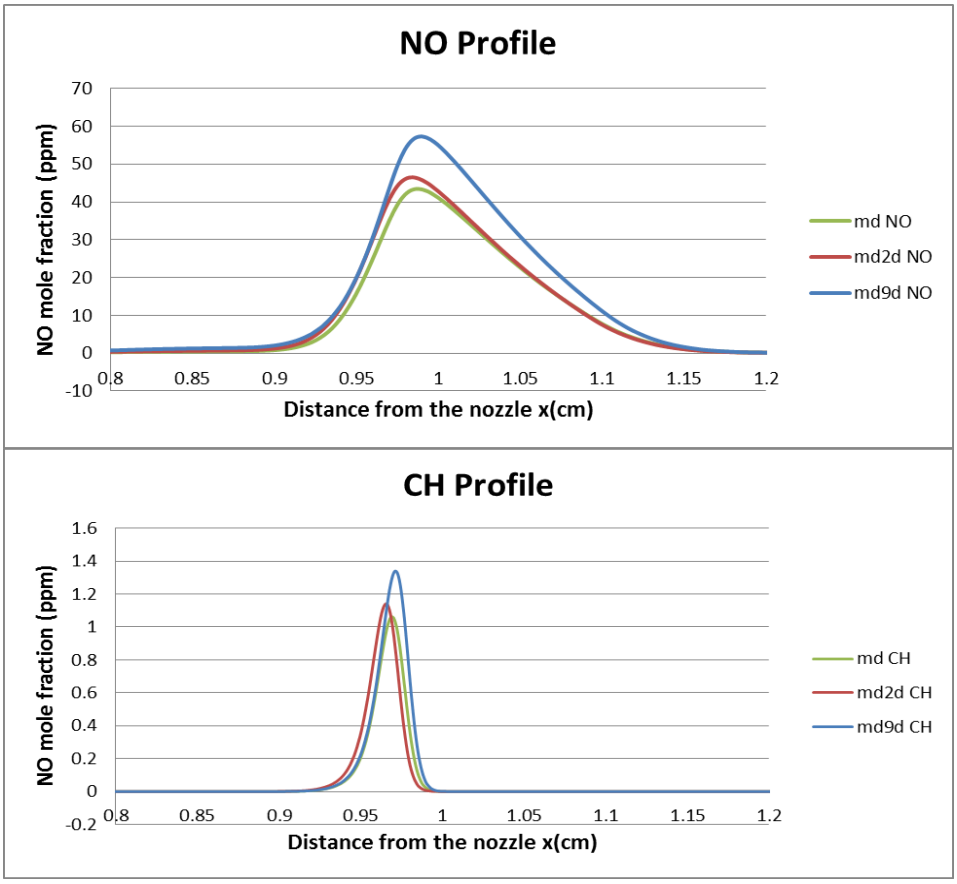

Figure 22: Comparison of NO and CH species profiles in a counter-flow diffusion flame formed by methyl decanoate (md), methyl-2-decenoate (MD2D), and methyl-9-decenoate (MD9D), respectively.

4. Conclusions

4.1 Summary

We have numerically investigated the flame structure and NO_x and PAH emissions in triple flames burning prevaporized n-heptane and 1-heptene fuels, which, respectively, represent the hydrocarbon side chain of the two surrogate biodiesel esters, methyl-octanoate (C9:0) and methyl-octenoate (C9:1). The objective is to examine the effect of unsaturated (double) bond in the fuel molecular structure on NO_x and soot emissions in a flame environment containing regions of lean premixed, rich premixed and non-premixed combustion. A validated detailed kinetic model with 198 species and 4932 reactions has been used to simulate triple flames with different levels of premixing at a fixed global equivalence ratio, and different strain rates. Important observations are as follows.

1. While the global structures of n-heptane and 1-heptene triple flames are similar, there are significant differences with respect to NO_x emission from these flames. For all the cases simulated, the NO_x emission from 1-heptene flames is higher than that from n-heptane flames. The NO production rates in each of the three reaction zones, i.e., the rich premixed, lean premixed, and non-premixed zones, are also higher in 1-heptene flames compared to n-heptane flames. Moreover, these differences become more pronounced as the level of premixing is increased.

2. The NO_x formed through the prompt, thermal, N_2O, and NNH mechanisms is also higher in 1-heptene triple flames compared to that in n-heptane triple flames. NO_x formation in the rich premixed zone is primarily due to the prompt NO, while that in the nonpremixed zone is mainly through the thermal route. In contrast, NO_x in the lean premixed zone is formed mostly through the NNH and N_2O mechanisms.

3. PAH species such as benzene, naphthalene, and pyrene are mostly formed in the rich premixed zone, and their emissions are significantly higher in 1-heptene flames than in n-heptane flames. The reaction pathway analysis indicated that the dominant path for benzene formation involves the combination of two propargyl (C_3H_3) radicals, and the presence of double bond in 1-heptene provides a significant route for its production through the formation of C_3H_5. This path is not favored in the high temperature oxidation of n-heptane, as it decomposes directly to smaller alkyl radicals.

4. As the level of premixing level is reduced, NO_x emissions decrease while PAH emissions increase. In addition, the relative contribution of thermal NO decreases, those of prompt and NNH mechanisms increase, and that of N_2O remains about the same, as the level of premixing is reduced.

5. As the strain rate is increased, the total NO emissions first increase due to the increased interaction between the nonpremixed and premixed reaction zones, but subsequently decrease due to the reduced residence time at higher strain rate. Also the relative contribution of prompt NO to total NO_x increases compared to that of thermal NO. While the PAH emissions decrease with the increase in strain rate, they are significantly higher in 1-heptene flames than in -heptane flames, irrespective of the strain rate.

6. The effect of double bond, strain rate, and premixing level has greater effect on larger PAH species.

7. With the presence of methyl ester group, methyl decenoate has a higher NO emission than methyl decanoate. The effect of the position of the double bond on NO emissions is still unclear.

4.2 Future research outlook

While it is well known that unsaturated biodiesel fuels produce higher amount of NO, there are other aspects that can vary the NO emissions in IC engines, e.g. ignition delay, premixing, flame temperature. The long chain unsaturated hydrocarbons have higher ignition delays than the saturated ones. Moreover, the isomers of such hydrocarbons, depending on the position of double bond in the carbon chain, have significantly different ignition delays. This makes it more complicated to analyze the reasons of the variation in NO emissions in IC engines. Future work can be in two directions. One is to further study other biodiesel surrogates in simple reactors like counter-flow configuration. Besides, it is also meaningful to conduct engine simulation with these biodiesel surrogates or as blends to further understand the overall effect of their chemistry on NO_x and PAH emissions.

Reference

(1) Song, H.; Tompkins, B.T.; Bittle, J.A.; Jacobs, T.J. Comparisons of NO emissions and soot concentrations from biodiesel-fuelled diesel engine. *Fuel* http://dx.doi.org/10.1016/j.fuel.2012.01.004

(2) Graboski, M.; McCormick, R.; Combustion of fat and vegetable oil derived fuels in diesel engines. *Prog. Energy Combust. Sci.* **1998**, 24, 125–164.

(3) McCormick, R.L.; Graboski, M.S.; Alleman, T.L.; Herring, A.M.; Tyson, K.S. Impact of biodiesel source material and chemical structure on emissions of criteria pollutants from a heavy-duty engine. *Environ. Sci. Technol.* **2001**, 35(9), 1742–1747.

(4) Lapuerta M.; Armas, O.; Rodríguez-Fernández, J. Effect of the alcohol type used in the production of waste cooking oil biodiesel on diesel performance and emissions. *SAE* Paper NO. 2008-01-1676, **2008**.

(5) Puhan, S.; Saravanan, N.; Nagarajan, G.; Vedaraman, N. Effect of biodiesel unsaturated fatty acid on combustion characteristics of a DI compression ignition engine. *Biomass and Bioenergy* **2010**, 34, 1079-1088.

(6) Schönborn, A.; Ladommatos, N.; Williams, J.; Allan, R.; Rogerson, J. The influence of molecular structure of fatty acid monoalkyl esters on diesel combustion. *Combust. Flame* **2009**, 156, 1396–1412.

(7) Benjumea, P.; Agudelo, J.R.; Agudelo, A.F. Effect of the degree of unsaturation of biodiesel fuels on engine performance, combustion characteristics, and emissions. *Energy Fuels* **2011**, 25 (1), 77–85.

(8) Salamanca, M.; Mondragón, F.; Agudelo, J. R.; Benjumea, P.; Santamaría, A. Variations in the chemical composition and morphology of soot induced by the unsaturation degree of biodiesel and a biodiesel blend. *Combust. Flame* **2012**, 159, 1100-1108.

(9) Garner, S.; Brezinsky, K. Biologically derived diesel fuel and NO formation: An experimental and chemical kinetic study, Part 1 *Combust. Flame* **2011**, 158, 2289-2301.

(10) Garner, S.; Dubois, T.; Togbe, C.; Chaumeix, N.; Dagaut, P.; Brezinsky, K. Biologically derived diesel fuel and NO formation: Part 2: Model development and extended validation. *Combust. Flame* **2011**, 158, 2302-2313.

(11) Garner, S.; Sivaramakrishnan, R.; Brezinsky, K. The high-pressure pyrolysis of saturated and unsaturated C_7 hydrocarbons. *Proc. Combust. Inst.* **2009**, 32, 461−467.

(12) Sarathy, S.M.; Gaïl, S.; Syed, S.A.; Thomson, M.J.; Dagaut, P. A comparison of saturated and unsaturated C_4 fatty acid methyl esters in an opposed flow diffusion flame and a jet stirred reactor. *Proc. Combust. Inst.* **2007**, 31, 1015–1022.

(13) Fu, X.; Garner, S.; Aggarwal, S.K.; Brezinsky, K. A numerical Study of NO_x emissions from n-heptane and 1-heptene counterflow flames. *Fuels* **2012**, 26, 879-888.

(14) Berta, P.; Puri, I.K.; Aggarwal, S.K. Structure of partially premixed n-heptane-air counterflow flames. *Proc. Combust. Inst.* **2005**, 30, 447-453.

(15) Berta, P.; Aggarwal, S.K.; Puri, I.K. An experimental and numerical investigation of n-heptane/air counterflow partially premixed flames and emission of NO_x and PAH species. *Combust. Flame* **2006**, 145, 740-764.

(16) Guo, H.; Smallwood, G.J. A numerical investigation on NO_x formation in counterflow n-heptane triple flames. *Int. J. Thermal Sci.* **2007**, 46, 936-943.

(17) Smallbone, A.J.; Liu, W.; Law, C.K.; You, X.Q.; Wang, H. Experimental and modeling study of laminar flame speed and non-premixed counterflow ignition of n-heptane. *Proc. Combust. Inst.* **2009**, 32, 1245-1252.

(18) Xue, H.; Aggarwal, S.K. NO_x emissions in n-heptane/air partially premixed flames. *Combust. Flame* **2003**, 132, 723-741.

(19) Cha, M.S.; Chung, S.H. *Symp. (Int.) Combust.* **1996**, 26, 121-128.

(20) Ghosal, S.; Vervisch, L. Stability diagram for lift-off and blowout of a round jet laminar diffusion flame. *Combust. Flame* **2001**, 123, 646-655.

(21) Chomiak, J.; Karlsson, A. Flame liftoff in diesel sprays. *Symp. (Int.) Combust.* **1996**, 26, 2557-2564.

(22) Mansour, M.S. Stability characteristics of lifted turbulent partially premixed jet flames. *Combust. Flame* **2003**, 133, 263-274.

(23) Joedicke, A.; Peters, N.; Mansour, M. The stabilization mechanism and structure of turbylent hydrocarbon lifted flames. *Proc. Combust. Inst.* **2005**, 30, 901-909.

(24) Kong, S.C.; Reitz, R.D. Application of detailed chemistry and CFD for predicting direct injection HCCI engine combustion and emissions. *Proc. Combust. Inst.* **2002**, 29, 663-669.

(25) Babajimopoulos, A.; Assanis, D.N.; Flowers, D.L.; Aceves, S.M.; Hessel, R.P. A fully coupled computational fluid dynamics and multi-zone model with detailed chemical kinetics for the simulation of premixed charge compression ignition engines. *Int. J. Engine Res.* **2005**, 6, 497-512.

(26) Briones, A.M.; Som, S.; Aggarwal, S.K. Effects of H_2 enrichment on the propagation characteristics of CH_4-air triple flames. *Combust. Flame* **2007**, 149, 448-462.

(27) Herbinet, O.; Pitz, W.J.; Westbrook, C.K. Detailed chemical kinetic oxidation mechanism for a biodiesel surrogate. Combust. Flame 2008, 154, 507-528.

(28) Lutz, A.E.; Kee, R.J.; Grear, J.F.; Rupley, F.M. *Sandia National Lab.* Report No. SAND96-8243.

(29) Kee, R.J.; Rupley, F.M.; Miller, J.A. *Sandia National Lab.* Report No. 89-8009B.

(30) Ranzi, E.; Dente, M.; Goldaniga, A.; Bozzano, G.; Faravelli, T. Lumping procedures in detailed kinetic modeling of gasification, pyrolysis, partial oxidation and combustion of hydrocarbon mixtures. *Prog. Energy Combust. Sci.* **2001**, 27, 99−139.

(31) Goldaniga, A.; Faravelli, T.; Ranzi, E. The kinetic modeling of soot precursors in a butadiene flame. *Combust. Flame* **2000**, 122, 350-358.

(32) Shimizu, T.; Williams, F.A.; Frassoldati, A. *Proceedings of the 43rd American Institute of Aeronautics and Astronautics (AIAA) Aerospace Science Meeting and Exhibit*; Reno, NV, Jan 10−13, **2005,** AIAA-0144.

(33) Frassoldati, A.; Faravelli, T.; Ranzi, E. Kinetic modeling of the interactions between NO and hydrocarbons at high temperature. *Combust. Flame* **2003**, 135, 97-112 .

(34) Miller, J.A.; Bowman, C.T. Mechanism and modeling of nitrogen chemistry in combustion. *Prog. Energy Combust.Sci.* **1989**, 15, 287–338.

(35) Bozzelli, J.W.; Dean, A.M. O+NNH: A possible new route for NO_x formation in flames. *Int. J. Chem. Kinetics* **1995**, 27, 1097-1109.

(36) Rørtveit, G.J.; Hustad, J.E.; Li, S.C.; Williams, F.A. Effects of diluents on NO_x formation in hydrogen counterflow flames. *Combust. Flame* **2002**, 130, 48-61.

(37) Guo, H.; Smallwood, G.J.; Liu, F.; Ju, Y.; Gülder, Ö.L. The effect of hydrogen addition on flammability limit and NO_x emission in ultra-lean counterflow CH_4/air premixed flames. *Proc. Combust. Inst.* **2005**, 30, 303-311.

(38) Löffler, G.; Sieber, R.; Harasek, M.; Hofbauer, H.; Hauss, R.; Landauf, J. *Fuel* NO_x formation in natural gas combustion—a new simplified scheme for CFD calculations. **2006**, 85, 513–523.

(39) Glarborg, P.; Alzueta, M.U.; Dam-Johansen, K.; Miller, J.A. Kinetic modeling of hydrocarbon/nitric oxide interactions in a flow reactor. *Combust. Flame* **1998**, 115, 1-27.

(40) Galletti, C.; Parente, A.; Derudi, M.; Rota, R.; Tognotti, L. Numerical and experimental analysis of NO emissions from a lab-scale burner fed with hydrogen-enriched fuels and operating in MILD combustion. *Int. J. Hydrogen Energy* **2009**, 34, 8339-8351.

(41) Konnov, A.A.; Colson, G.; Ruyck, J.D. NO formation rates for hydrogen combustion in stirred reactors. *Fuel* **2001**, 80, 49-65.

(42) Luo, Z.; Plomer, M.; Lu, T.; Som, S.; Longman, D. E.; Sarathy S.M.; Pitz, W.J. A reduced mechanism for biodiesel surrogate for compression ignition engine applications. *Fuel* 2012, 99, 143-153.

(43) Heywood, J.B. *Int. Combust. Engine Fundament.*, McGraw-Hill, New York, **1988**.

(44) Guo, H.; Liu, F.; Smallwood, G.J. A numerical study of laminar methane/air triple flames in two-dimensional mixing layers. *Int. J. Thermal Sci.* **2006**, 45, 586–594.

(45) Yamamoto M.; Duan S.; Senkan S. The effect of strain rate on polycyclic aromatic hydrocarbon (PAH) formation in acetylene diffusion flames. *Combust. Flame* **2007**, 151, 532-541.

(46) Zhang, R.H.; Eddings, E.G.; Sarofim. A.F. A Journey from n-Heptane to Liquid Transportation Fuels. 1. The Role of the Allylic Radical and Its Related Species in Aromatic Precursor Chemistry. *Energy Fuels* 2008, 22 (2), 945–953.

(47) Zhang, R.H.; Eddings, E.G.; Sarofim. A.F. Olefin Chemistry in a Premixed n-Heptane Flame. *Energy Fuels* 2007, 21 (2), 677–685.

(48) Zhang, R.H.; Eddings, E.G.; Sarofim. A.F.; Westbrook, C.K. Mechanism Reduction and Generation Using Analysis of Major Fuel Consumption Pathways for n-Heptane in Premixed and Diffusion Flames. *Energy Fuels* 2007, 21 (4), 1967-1976.

(49) Miller, J.A.; Melius, C.F. Kinetic and thermodynamic issues in the formation of aromatic compounds in flames of aliphatic fuels. *Combust. Flame* **1992**, 91, 21-39.

VITA

NAME	Sudhanshu Jain
EDUCATION	B.E., Automation, Southeast University, China, 2008
EXPERIENCE	Research Aid, the Energy System Laboratory, Mechanical and Industrial Engineering, University of Illinois at Chicago, Chicago, Illinois, 2011-2012
	Teaching Assistant, Mechanical and Industrial Engineering, University of Illinois at Chicago, Chicago, Illinois, 2011-2012
	Assistant Engineer, Dalian Datang Scientific Instruments Co., Ltd Dalian, China, 2008-2010
PUBLICATIONS	"A Numerical Investigation of NOx Emissions from n-Heptane and 1-Heptene Triple Flames", *Spring Technical Meeting of the Central States Section of Combustion Institute*, 2012 "A Numerical Investigation of NOx and PAH Emissions from n-Heptane and 1-Heptene Triple Flames" Submitted to *Energy & Fuels*, 2012.